CP–HISQC: A better version of HSQC experiment for intrinsically disordered proteins under physiological conditions

ARTICLE *in* JOURNAL OF BIOMOLECULAR NMR · FEBRUARY 2014

Impact Factor: 3.14 · DOI: 10.1007/s10858-014-9815-5 · Source: PubMed

2 AUTHORS:

Tairan Yuwen
Purdue University
7 PUBLICATIONS **47** CITATIONS
SEE PROFILE

Nikolai Skrynnikov
Purdue University
59 PUBLICATIONS **2,396** CITATIONS
SEE PROFILE

J Biomol NMR (2014) 58:175–192
DOI 10.1007/s10858-014-9815-5

ARTICLE

CP-HISQC: a better version of HSQC experiment for intrinsically disordered proteins under physiological conditions

Tairan Yuwen · Nikolai R. Skrynnikov

Received: 18 November 2013 / Accepted: 24 January 2014 / Published online: 5 February 2014

Abstract ^{1}H–^{15}N HSQC spectroscopy is a workhorse of protein NMR. However, under physiological conditions the quality of HSQC spectra tends to deteriorate due to fast solvent exchange. For globular proteins only a limited number of surface residues are affected, but in the case of intrinsically disordered proteins (IDPs) HSQC spectra are thoroughly degraded, suffering from both peak broadening and loss of intensity. To alleviate this problem, we make use of the following two concepts. (1) Proton-decoupled HSQC. Regular HSQC and its many variants record the evolution of multi-spin modes, $2N_xH_z$ or $2N_xH_x$, in indirect dimension. Under the effect of fast solvent exchange these modes undergo rapid decay, which results in severe line-broadening. In contrast, proton-decoupled HSQC relies on N_x coherence which is essentially insensitive to the effects of solvent exchange. Moreover, for measurements involving IDPs at or near physiological temperature, N_x mode offers excellent relaxation properties, leading to very sharp resonances. (2) Cross-polarization ^{1}H-to-^{15}N transfer. If CP element is designed such as to lock both $^{1}H^{N}$ and water magnetization, the following transfer is effected: $H_x^{water} \rightarrow H_x^N \rightarrow N_x$. Thus water magnetization is successfully exploited to boost the amount of signal. In addition, CP element suffers less loss from solvent exchange, conformational exchange, and dipolar relaxation compared to the more popular INEPT element. Combining these two concepts, we have implemented the experiment termed CP-HISQC (*c*ross-*p*olarization assisted *h*eteronuclear *i*n-phase *s*ingle-*q*uantum *c*orrelation). The pulse sequence has been designed such as to preserve water magnetization and therefore can be executed with reasonably short recycling delays. In the presence of fast solvent exchange, $k_{ex} \sim 100\ s^{-1}$, CP-HISQC offers much better spectral resolution than conventional HSQC-type experiments. At the same time it offers up to twofold gain in sensitivity compared to plain proton-decoupled HSQC. The new sequence has been tested on the sample of drkN SH3 domain at pH 7.5, 30 °C. High-quality spectrum has been recorded in less than 1 h, containing resonances from both folded and unfolded species. High-quality spectra have also been obtained for arginine side-chain $H^{\varepsilon}N^{\varepsilon}$ groups in the sample of short peptide Sos. For Arg side chains, we have additionally implemented (HE)NE(CD)HD experiment. Using ^{13}C-labeled sample of Sos, we have demonstrated that proton-to-nitrogen CP transfer remains highly efficient in the presence of solvent exchange as fast as $k_{ex} = 620\ s^{-1}$. In contrast, INEPT transfer completely fails in this regime.

Keywords ^{1}H–^{15}N correlation spectroscopy · Proton-decoupled HSQC · Cross-polarization · Amide solvent exchange · Intrinsically disordered proteins · Arginine side-chain $H^{\varepsilon}N^{\varepsilon}$ group

Electronic supplementary material The online version of this article (doi:10.1007/s10858-014-9815-5) contains supplementary material, which is available to authorized users.

T. Yuwen · N. R. Skrynnikov (✉)
Department of Chemistry, Purdue University, West Lafayette, IN 47907, USA
e-mail: nikolai@purdue.edu

N. R. Skrynnikov
Laboratory of Biomolecular NMR, St. Petersburg State University, St. Petersburg 199034, Russia

Introduction

Two-dimensional ^{1}H–^{15}N correlation spectroscopy is the most widely used class of experiments in the field of protein NMR. There are a number of reasons for continued popularity of these experiments. Bacterially expressed recombinant proteins with ^{15}N labeling can be produced using conventional protocols at very little extra cost. HSQC-type experiments generally have high sensitivity and yield the spectra that are well dispersed and free from interference of the water signal. Furthermore, these spectra are exquisitely sensitive to changes in protein status, such as ligand binding or conformational rearrangements. The HSQC-based sequences are also used to measure ^{15}N relaxation rates, paramagnetic relaxation enhancements, residual dipolar couplings, and other experimental parameters of prime importance.

For all of its strengths, ^{1}H–^{15}N correlation spectroscopy is not ideally suited for measurements at or near physiological conditions (pH 7.4, 37 °C). Under these conditions the quality of the spectra deteriorates due to rapid $^{1}H^{N}$ solvent exchange which causes both loss of intensity and line broadening. In the case of folded soluble proteins only those amides that lie on the surface of the protein and have a significant degree of solvent exposure are affected. However, among these affected residues one often finds key catalytic residues, as well as residues which are critically important for ligand binding (Mueller et al. 2001; Amezcua et al. 2002; Haddad et al. 2005). A similar situation is encountered in the samples of membrane proteins reconstituted in lipids or detergents; in this case solvent exchange has an effect on water-exposed loops (Fernandez et al. 2004). Of particular importance for our study, solvent exchange can have severe adverse impact on ^{1}H–^{15}N spectroscopy of intrinsically disordered proteins (IDPs). The degree of water exposure is typically very high for most residues in IDPs. As a consequence, already at room temperature and pH 6.0 the quality of the spectra visibly deteriorates. This happens regardless of residual secondary structure. Indeed, the presence of transient, low-populated α-helices or β-turns offers little protection against solvent exchange (Croke et al. 2008; Hsu et al. 2009; Gray et al. 2012). Even in the case of molten globule proteins, solvent exchange can thoroughly degrade the quality of ^{1}H–^{15}N spectra (Loh et al. 1995).

In principle, the problems associated with solvent exchange can be avoided if one resorts to pulse sequences employing non-labile protons or heteronuclei. A number of experiments have been developed along these lines including, notably, ^{13}C-based experiments (Bermel et al. 2006; Pasat et al. 2008; Felli and Brutscher 2009; Werbeck et al. 2013). However, given the substantial cost of ^{13}C-labeling and low sensitivity of the proton-less pulse schemes, the ^{1}H–^{15}N spectroscopy remains the first choice for NMR studies of IDPs.

It has been recognized early on that in the presence of moderately fast solvent exchange it is important to preserve water magnetization (Grzesiek and Bax 1993; Farrow et al. 1994). Along these lines van Zijl and co-workers developed FHSQC sequence, which offers excellent water preservation properties (Mori et al. 1995). Transfer of magnetization from water to labile protein sites makes it possible to relatively quickly replenish $^{1}H^{N}$ magnetization. As a result, FHSQC experiment can be executed with relatively short recycling delays. The same is true for the more recent SOFAST-HMQC experiment (Schanda and Brutscher 2005). The superior performance of SOFAST-HMQC under moderately fast exchange conditions, $k_{ex} \sim 1$–$10\ s^{-1}$, has been recently documented (Yao et al. 2011).

While the experiments such as FHSQC and SOFAST-HMQC offer superior sensitivity, they also suffer from one potential setback. Specifically, these sequences utilize multispin modes such as $2N_xH_z$ or $2N_xH_x$ to record the evolution in t_1 domain. Under the effect of solvent exchange, such multispin modes undergo rapid decay, resulting in dramatic line broadening (Skrynnikov and Ernst 1999). As a result, the increased solvent exchange leads to loss of spectral resolution in nitrogen dimension.

This problem has been addressed in another pulse sequence, which has been originally termed proton-decoupled HSQC (Bax et al. 1990). This experiment relies on N_x coherence to record the evolution in t_1 domain. In the presence of robust proton decoupling, N_x evolves essentially independently of solvent exchange. In the case of highly mobile disordered protons, the spectra can be recorded with very narrow linewidth in ^{15}N dimension. The favorable properties of proton-decoupled HSQC with respect to solvent exchange have been pointed out already in the original report (Bax et al. 1990). Later the same strategy has been used to record the spectra of lysine side-chain NH_3 groups, which are otherwise difficult to observe due to the fast solvent exchange (Iwahara et al. 2007). The lysine experiment was termed *h*eteronuclear *i*n-phase *s*ingle *q*uantum *c*oherence spectroscopy or HISQC. Very recently, we have used this scheme in the context of ^{15}N R_2 measurements in IDPs (Yuwen and Skrynnikov 2013).

In this report we present the proton-decoupled HSQC experiment which uses cross-polarization (CP) element as a starting point. The new pulse sequence is termed CP-HISQC. As demonstrated below, the CP element makes efficient use of water magnetization, achieving the following transfer:

$$H_x^{water} \xrightarrow{k_{ex}} H_x^{N} \xrightarrow{^{1}J_{HN}} N_x \qquad (1)$$

For the sample conditions close to physiological the use of the CP scheme affords significant gain in sensitivity

compared to the previously reported HISQC sequence. At the same time, CP-HISQC offers dramatically improved spectral resolution compared to conventional experiments such as FHSQC and SOFAST-HMQC. The combination of superior resolution and good sensitivity makes CP-HISQC sequence particularly well-suited for studies of IDPs at or near physiological conditions. It can also be useful for studies of globular proteins (membrane proteins) if the goal is to capture the signals from surface sites undergoing rapid solvent exchange.

Setting up the experiment is sufficiently easy, and the efficient CP transfer is achieved simultaneously for those residues that experience fast solvent exchange and for those residues that are protected. This property has been demonstrated on the sample of N-terminal SH3 domain of adaptor protein drk, which contains both folded and unfolded forms of the protein (Farrow et al. 1995). Using CP-HISQC sequence we have recorded a high-quality backbone $^{1}H^{N}$–^{15}N spectrum of drkN SH3 at 30 °C, pH 7.5. In addition, we have also recorded arginine side-chain $^{1}H^{\varepsilon}$–$^{15}N^{\varepsilon}$ spectra of ten-residue peptide from guanine nucleotide exchange factor Sos (Wu et al. 1995). These data were collected at pH 6.0 in the range of temperatures from 23 to 37 °C. Using the sample of Sos peptide we have also shown that CP transfer remains efficient even in the presence of very fast solvent exchange (50 °C, $k_{ex} \sim 600\ s^{-1}$).

Results

CP-HISQC pulse sequence

The new pulse sequence CP-HISQC (*c*ross-*p*olarization assisted *h*eteronuclear *i*n-phase *s*ingle-*q*uantum *c*orrelation) is shown in Fig. 1. The initial hard ^{1}H 90° pulse followed by high-power DIPSI-2 pulse train lock both amide and water magnetization along the x axis. As amides undergo solvent exchange, the H_x magnetization on amides is gradually replaced with H_x magnetization from water. At the same time H_x is continuously transformed into N_x via the cross-polarization transfer. The ability of the CP

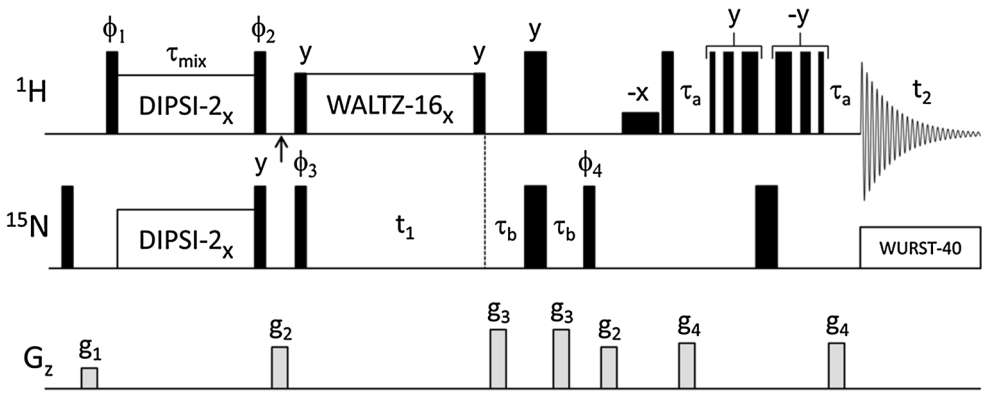

Fig. 1 CP-HISQC pulse sequence for ^{1}H–^{15}N correlation spectroscopy. The parameters below are for backbone amide measurements using the sample of drkN SH3 (unless indicated otherwise). Proton carrier is initially placed at the middle of the amide region, 8.20 ppm. At the point indicated by vertical arrow, the carrier is jumped to water resonance, 4.71 ppm. Hard 90° proton pulses have duration 6.1 μs. 90° water flip-back pulse has rectangular shape and duration 880 μs. DIPSI-2 cross-polarization element (Rucker and Shaka 1989) uses 4.0 kHz *rf* field on both channels (corresponding to 90° pulses of duration 62 μs). WALTZ-16 decoupling (Shaka et al. 1983) is applied with *rf* field strength 5.0 kHz (the same as for the flanking 90° pulses). This is sufficient to minimize the loss of N_x coherence due to solvent exchange (scalar relaxation) (Yuwen and Skrynnikov 2013). Nitrogen carrier has been set at 119 ppm. Hard ^{15}N pulses are of duration 38 μs. WURST-40 decoupling (Kupce and Freeman 1996) during the acquisition period uses *rf* field strength 0.6 kHz. The durations of delays $\tau_a = 0.8 \times 1/(4J_{NH}) = 2.15$ ms and $\tau_b = 0.9 \times 1/(4J_{NH}) = 2.40$ ms have been optimized based on the model calculations assuming $k_{ex} = 100\ s^{-1}$. The duration of the CP element τ_{mix} is (3/2) × T_{DIPSI2}, where T_{DIPSI2} is the length of full DIPSI-2 cycle corresponding to 10360° rotation. This translates into $\tau_{mix} = 10.705$ ms, as used in the actual experiment. The spacing between the consecutive pulses in 3-9-19 WATERGATE (Sklenar et al. 1993) is 183 μs. The phase cycle employed is: $\phi_1 = y, -y$; $\phi_2 = -y, y$; $\phi_3 = 2(y), 2(-y)$; $\phi_4 = 4(x), 4(-x)$; $\phi_{rec} = x, -x, -x, x, -x, x, x, -x$. DIPSI-2 and WALTZ-16 sequences are applied with (initial) phase x. The TPPI scheme is implemented by inverting ϕ_4 in concert with ϕ_{rec} (Marion et al. 1989). Quadrature detection in F_1 is achieved by incrementing ϕ_4 by π/2. Four scans per t_1 increment are sufficient to obtain high-quality spectra free from any artefacts. Gradient strengths in G/cm (length in ms) are: $g_1 = 5.0$ (1.0), $g_2 = 10.0$ (1.0), $g_3 = 15.0$ (1.25), $g_4 = 11.0$ (1.0). We choose not to employ the enhanced sensitivity scheme (Palmer et al. 1991; Kay et al. 1992) since it requires ca. extra 5 ms transfer time, which translates into significant loss of signal in the presence of solvent exchange with $k_{ex} \sim 100\ s^{-1}$. When recording $^{1}H^{\varepsilon}$–$^{15}N^{\varepsilon}$ correlation map for Arg side chains, proton *rf* carrier is initially placed in $^{1}H^{\varepsilon}$ region, 7.2 ppm, and then jumped to water. Nitrogen carrier is positioned at 85 ppm. The $^{1}H^{\varepsilon}$–$^{15}N^{\varepsilon}$ spectra have been recorded using ^{13}C-labeled sample of peptide Sos. To suppress J_{NC} evolution, a composite ($90^{\circ}_{y}180^{\circ}_{x}90^{\circ}_{y}$) carbon pulse has been inserted in the middle of the t_1 evolution period (net duration 66 μs, *rf* carrier at 118 ppm). Other settings, including the CP element, are the same as in the backbone experiment

element to efficiently utilize the influx of new water magnetization is the key to its superior performance.

Following the CP element, N_x magnetization is ^{15}N-frequency-labeled during the evolution period t_1, while proton decoupling is applied to suppress $^1J_{NH}$ and thus prevent the build-up of anti-phase magnetization. The use of the in-phase nitrogen magnetization greatly improves the quality of the spectra compared to the standard scheme (where $2N_xH_z$ evolves during t_1, suffering dramatic losses due to rapid solvent exchange). Following the evolution period, refocused INEPT is used to return magnetization to amide protons for detection. While CP scheme is strongly preferred for the initial proton-to-nitrogen transfer, the reverse transfer is best accomplished using INEPT (the practical considerations dictating this choice are discussed below).

Special care has been taken to preserve water magnetization throughout the pulse sequence. As already pointed out, water magnetization is locked during the CP element; likewise, it is locked during t_1 period by means of the WALTZ sequence of phase x. Finally, during the refocused INEPT water magnetization is maintained along the z axis. As a result, at the end of each scan water retains ca. 75 % of its equilibrium magnetization, which is then quickly transferred to amide sites through solvent exchange. In this manner we avoid long recycling delays which would otherwise be necessary to allow for recovery of water magnetization.

The sequence shown in Fig. 1 is similar to the well-known proton-decoupled HSQC experiment (Bax et al. 1990), as well as more recent HISQC experiment (Iwahara et al. 2007) developed for Lys side-chain NH_3 groups. The main distinction of our sequence is the use of the CP element which leads to significantly better sensitivity (see below). We have also found that 3-9-19 WATERGATE (Sklenar et al. 1993) offers better water preservation compared to the version employing 90° selective rectangular pulses (Iwahara et al. 2007).

The CP element has been designed such as to lock both water and $^1H^N$ magnetization along the x axis. We have determined that optimal results are obtained when (i) carrier is set on $^1H^N$ and (ii) the strength of DIPSI *rf* field is at least two times greater than the frequency offset between $^1H^N$ and water, $\nu_1^H/\Delta \geq 2.0$. In principle, increasing the strength of *rf* field beyond this level is useful, but the gains tend to level off (discussed in what follows).

Strictly speaking, the *rf* field strength $\nu_1^H = 2\Delta$ is insufficient to properly align water magnetization along the x axis. Following the initial hard 90° pulse, water magnetization lands on the x axis. Subsequently, under the effect of off-resonance DIPSI, water magnetization travels on a complicated trajectory on the surface of a unit sphere (while maintaining a significant x projection). This situation can be described in terms of water magnetization being partially locked. After full DIPSI-2 cycle is completed, water is returned to the x axis, reflecting excellent offset compensation properties of the DIPSI-2 composite pulse. At this point the second hard 90° pulse is applied, returning water magnetization to the z axis. This scheme ensures good preservation of water magnetization, which is essential for the sensitivity of the measurements.

The necessary condition for this favorable scenario is that the length of the CP period, τ_{mix}, is proportional to the integer number of DIPSI-2 cycles. In practice, we have found that good results are obtained already with semi-integer number of DIPSI-2 cycles, $\tau_{mix} = (n/2) \times T_{DIPSI2}$. On the other hand, the length of τ_{mix} is dictated by the requirements of cross-polarization transfer. In the absence of solvent exchange, the optimal transfer is achieved when $\tau_{mix} = 1/J_{NH} = 10.8$ ms. How to reconcile these two requirements as per the length of τ_{mix}?

It turns out that in the presence of rapid solvent exchange high efficiency of the CP transfer is attained in a broad interval of τ_{mix}. Specifically, the range of τ_{mix} ca. 10–13 ms can be recommended (see Fig. 5 below). Within this range it is easy to accommodate the semi-integer number of DIPSI-2 cycles. For example, in our backbone drkN SH3 experiment we have used $\tau_{mix} = (3/2) \times T_{DIPSI2} = 10.705$ ms.

CP-HISQC spectra of $^{15}N^{\varepsilon}$–$^1H^{\varepsilon}$ groups from Arg side chains

Sos peptide with the primary sequence PPPVPPRRRR is a proline-rich fragment from guanine nucleotide exchange factor Sos. This fragment is responsible for the interaction with SH3 domains of various adaptor proteins (Wu et al. 1995). The signals from four arginine $^{15}N^{\varepsilon}$–$^1H^{\varepsilon}$ groups in Sos are largely overlapped; the spectrum contains two resolved peaks of unequal height (see Fig. 2, bottom row).

Solvent exchange rates for $^{15}N^{\varepsilon}$–$^1H^{\varepsilon}$ sites can be measured by means of the experiment that records $^{13}C^{\delta}$,$^1H^{\delta}$ correlation map (Segawa et al. 2008). In the case of Sos peptide, this spectrum features a single four-fold degenerate peak. As a consequence, k_{ex} constant obtained in this experiment represents an effective average of the four exchange rates. Given that four arginines are contiguously located at the C-terminus of the Sos peptide and are dynamically disordered, it is reasonable to assume that their individual exchange rates are all similar to each other and close to the experimentally measured k_{ex}. Using ^{13}C-labeled sample of Sos with pH 6.0 and pulse sequence adapted from (Segawa et al. 2008) we determined $^{15}N^{\varepsilon}$–$^1H^{\varepsilon}$ solvent exchange rate at three different temperatures: 43 s^{-1} at 23 °C, 86 s^{-1} at 30 °C, and 170 s^{-1} at 37 °C.

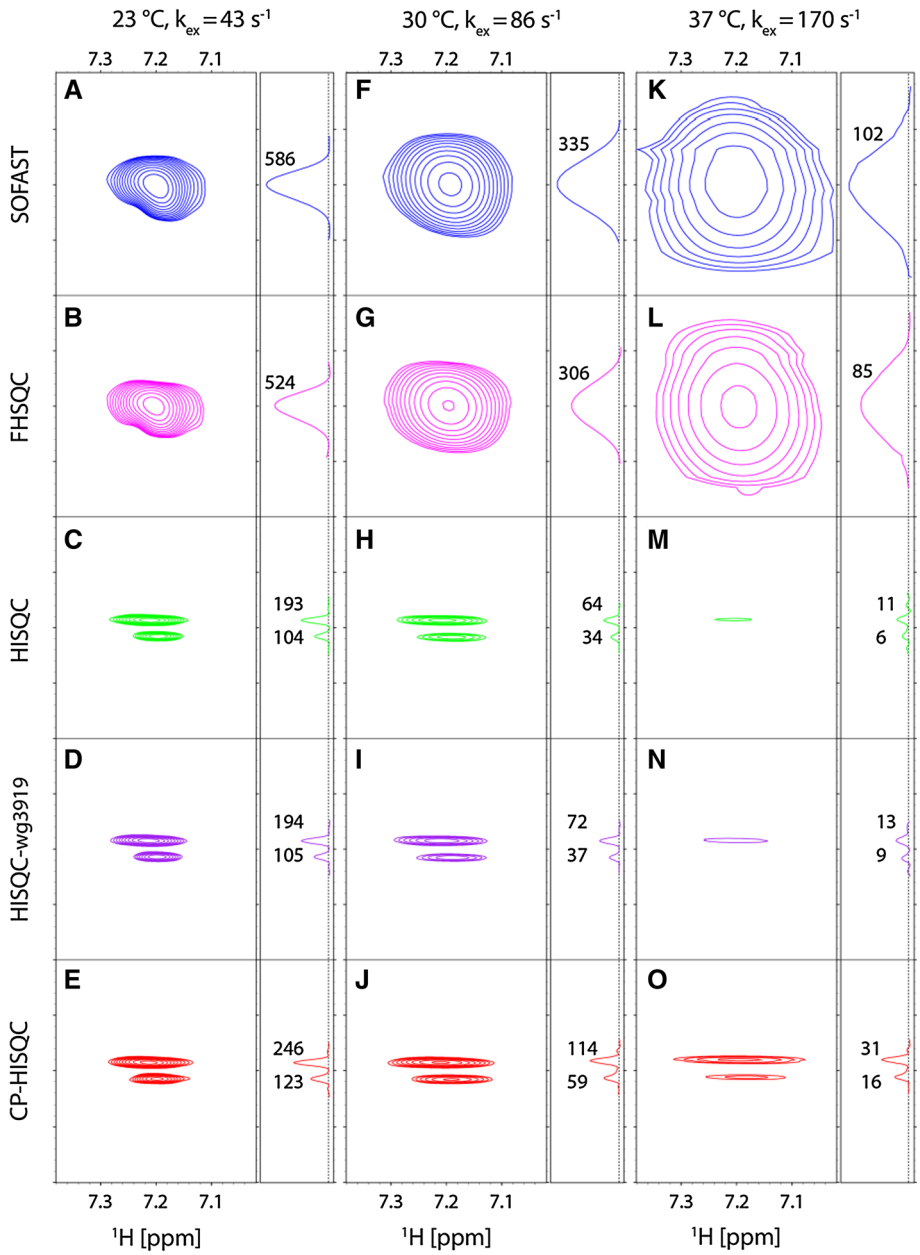

Fig. 2 Arginine $^{1}H^{\varepsilon}$–$^{15}N^{\varepsilon}$ correlation maps obtained for the sample of Sos peptide at three different temperatures using five different experimental schemes (as indicated in the plot). The durations of all experiments are approximately equal, ca. 10 min. The *side panels* show 1D cross-sections at 7.2 ppm; the number next to each peak indicates the corresponding S/N ratio. All spectra taken at the same temperature are plotted with the same scale. The separation between the two $^{15}N^{\varepsilon}$ resonances is 0.3 ppm

This range of k_{ex} is well suited for testing the performance of the new CP-HISQC experiment.

The $^{15}N^{\varepsilon}$–$^{1}H^{\varepsilon}$ spectral maps from the new CP-HISQC experiment have been compared with the spectra from four other popular experiments with optimized sensitivity and/or resolution: SOFAST-HMQC (Schanda et al. 2005), FHSQC (Mori et al. 1995), HISQC (Iwahara et al. 2007), and HISQC-wg3919 (our modification of the original HISQC sequence utilizing 3-9-19 WATERGATE element). The latter three experiments are specifically designed for samples with fast solvent exchange. All spectra were recorded using the recycling delays optimized for best signal-to-noise ratio: 0.2 s for SOFAST-HMQC and FHSQC, 1.0 s for HISQC, HISQC-wg3919, and CP-HISQC. When choosing the recycling delay for CP-HISQC, one should bear in mind that cross-polarization element creates a certain load on the probe (4.0 kHz ^{15}N *rf* field applied for 10.7 ms), although this is not a factor for the latest-generation probes which can easily handle such amount of power while requiring only short recycling delays (Ban et al. 2012). All experiments illustrated in Fig. 2 use the same INEPT delays, which have been optimized based on model calculations assuming $k_{ex} = 100\ s^{-1}$.

The data in Fig. 2 show that the SOFAST-HMQC and FHSQC sequences which rely on the evolution of two-spin coherences ($2N_xH_x$ and $2N_xH_z$, respectively) suffer from fast solvent exchange, causing broadening of spectral peaks in indirect dimension. In contrast, the three HISQC

sequences which record the evolution of in-phase coherence (N_x) produce much sharper signals. Given this distinctive behavior, we have set up the experiments such as to obtain optimal performance in relation to their intrinsic properties.

For simplicity let us focus on the data in the right column, where the effect of fast solvent exchange is especially prominent. The SOFAST-HMQC and FHSQC data shown in the right column have been recorded with only 4 increments in indirect dimension ($t_1 = 8$ ms); because of the rapid loss of magnetization there is no need in lengthy evolution period. The line broadening is extreme and the spectral resolution is poor, making it impossible to identify two distinct peaks separated by 0.3 ppm in ^{15}N dimension. Due to excellent water preservation properties, $^1H^\varepsilon$ magnetization is quickly replenished in these experiments. As a consequence, the data can be recorded with high repetition rate, which makes the experiments highly sensitive (cf. panels K and L in Fig. 2).

On the other hand, all three HISQC sequences have been recorded with 64 increments ($t_1 = 175$ ms). The decay of N_x magnetization is slow, which allows for long t_1 evolution and translates into high resolution in ^{15}N dimension. If desired, the resolution can be further improved by extending t_1 period, thus taking advantage of the fact that intrinsic ^{15}N R_2 relaxation in peptides and disordered proteins is typically very slow at the physiological temperature of 37 °C, on the order of 1 s^{-1}. In principle, along these lines one can obtain spectra with very sharp ^{15}N resonances, reminiscent of small molecules. Recording such spectra would require somewhat longer experimental time, ca. 1–2 h.

While HISQC experiments clearly display superior resolution, their sensitivity is a source of concern. A substantial amount of signal is lost due to solvent exchange during the refocused INEPT periods. Furthermore, the water preservation properties are not as good as in SOFAST experiment, which necessitates the use of longer recycling delays. All of this translates into mediocre sensitivity. The panel M in Fig. 2 illustrates arginine $^{15}N^\varepsilon$-$^1H^\varepsilon$ spectrum recorded by means of the HISQC sequence (Iwahara et al. 2007). The two peaks are borderline detectable, with S/N ratios of 11 and 6. Certain improvement can be obtained by implementing a better water preservation scheme. Specifically, we have found that 3-9-19 WATERGATE (Sklenar et al. 1993) achieves better results than the original version employing water flip-back pulses. To quantitate this (trivial) improvement, we have set up the experiment which is different from the original HISQC only in that it uses 3-9-19 WATERGATE (HISQC-wg3919). The obtained moderate improvement can be judged by examining the data in panel N.

Of greater interest, however, are the gains associated with the use of CP element to transfer magnetization from ^{1}H to ^{15}N. Replacing the first refocused INEPT period in the pulse sequence with CP element results in twofold gain in peak intensity (cf. panels N and O in Fig. 2). The S/N ratios of the two observed peaks are increased to 31 and 16. Of note, CP-HISQC is the only experiment which obtains a fully satisfactory spectrum in ca. 10 min, allowing for reliable detection of the two well-resolved peaks.

Finally it is worth pointing out that original HISQC sequence has been developed for lysine side-chain NH_3 groups; in these four-spin systems the maximum attainable efficiency for both refocused INEPT and CP element does not exceed 44 %. Note, however, that CP-HISQC retains its advantage over the regular HISQC also in this case. The application to arginine $H^\varepsilon N^\varepsilon$ sites discussed above is free of this limitation, and so is the application to backbone $H^N N$ sites, which is described in the next section.

CP-HISQC spectra of backbone amides

The N-terminal SH3 domain of the Drosophila adaptor protein drk (drkN SH3 domain) is a well-established model system for studies of protein disorder (Marsh and Forman-Kay 2009). The protein is marginally stable; in vitro it exists in a state of dynamic equilibrium between folded (F) and unfolded (U) forms. The exchange between the two states is slow, so that the spectra feature two distinct sets of peaks. From our perspective this is an attractive model for complex protein system, which combines the elements of order and disorder. Such complex systems increasingly become the focus of advanced NMR studies (Bista et al. 2012).

For our experimental measurements we have used the sample of drkN SH3 at pH 7.5, 30 °C. The proportion of F and U species under these conditions is approximately 1:1 (Zhang and Forman-Kay 1995). The unfolded form of drkN SH3 offers little protection against solvent exchange (Chevelkov et al. 2010). Therefore, it is appropriate to calculate solvent exchange rates using the simple algorithm which has been originally developed for random-coil peptides (Bai et al. 1993; Connelly et al. 1993). The results are dependent on protein primary sequence; for the unfolded drkN SH3, the majority of the predicted k_{ex} values fall in the range 15–150 s^{-1}. This is the regime where CP-HISQC is expected to be useful.[1]

In what follows we compare CP-HISQC with four other experiments that have been designed with fast solvent exchange in mind. Similar to the previous section, we have set up each experiment with consideration for its individual

[1] The alternative sample conditions could be pH 7.2, 37 °C. These conditions are relevant for cytosol (Orij et al. 2009). They give rise to very similar k_{ex} rates and are also suitable for CP-HISQC measurements.

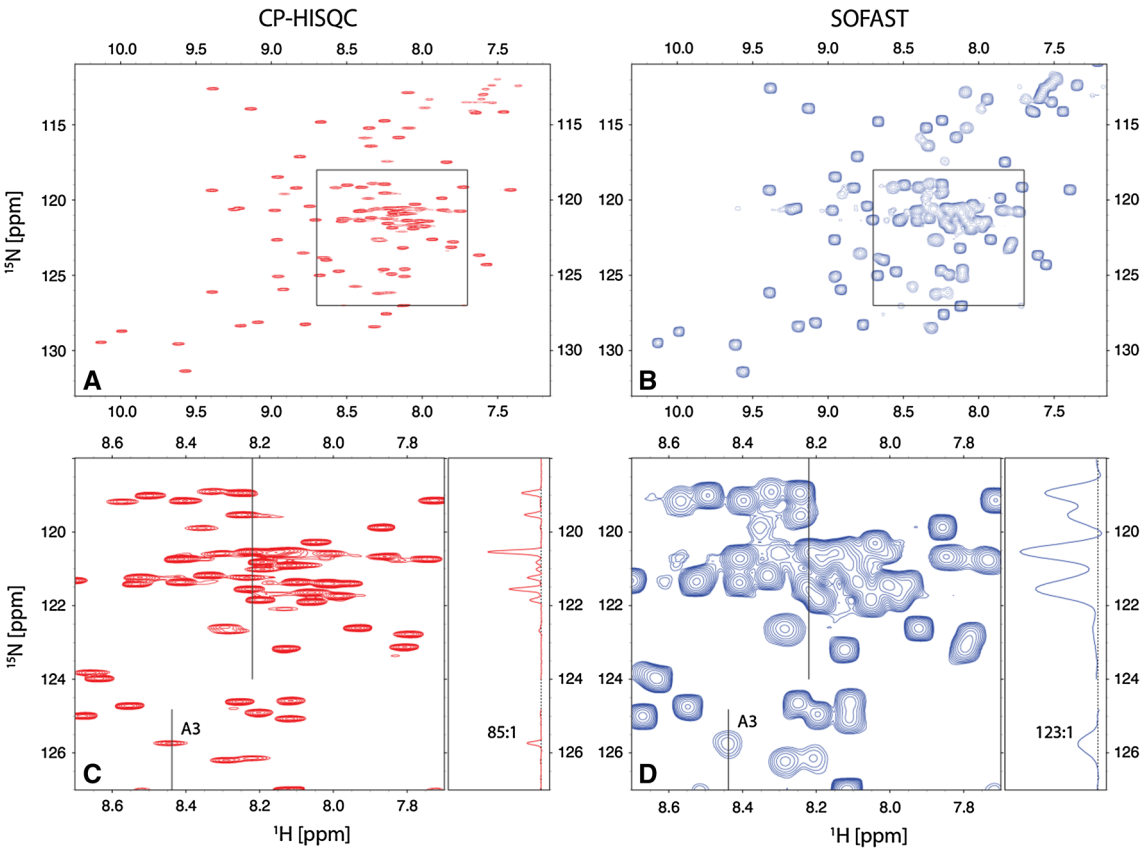

Fig. 3 (**a**, **b**) CP-HISQC and SOFAST-HMQC backbone amide spectra of drkN SH3. Each spectrum has been acquired in 50 min. The regions enclosed in rectangular boxes are magnified in panels (**c**, **d**). Black vertical lines indicate the position of 1D traces (displayed in *side panels*). The peak from residue A3 belonging to the unfolded form of drkN SH3 is labeled in the graph. For the purpose of plotting the spectra were scaled such that the noise level in all two-dimensional spectral maps is the same

properties. Specifically, SOFAST-HMQC and FHSQC have been recorded with 72 increments in indirect dimension, $t_1 = 39$ ms, and short recycling delays, $d_1 = 0.2$ s. At the same time, all HISQC experiments were recorded with 320 increments, $t_1 = 177$ ms, and standard recycling delay, $d_1 = 1.0$ s. Similar to the previous section, the best results have been obtained from SOFAST-HMQC (high sensitivity) and CP-HISQC (superior resolution in combination with reasonably good sensitivity). The corresponding spectra, both of which have been collected in ca. 50 min, are shown in Fig. 3.

The results in Fig. 3 demonstrate a dramatic improvement in resolution afforded by CP-HISQC experiment. The effect is especially obvious in panels C and D, which represent the most crowded portion of the spectrum. Indeed, a significant number of signals that are partially or fully overlapped in the SOFAST-HMQC spectrum turn out to be nicely resolved in CP-HISQC (cf. also 1D traces displayed in the side panels). This result is of major importance for studies of intrinsically disordered proteins or, more broadly, protein systems with elements of disorder. It is well known that the spectra of IDPs tend to be crowded and therefore high resolution is often key to the success of NMR studies. The increase in the number of quantifiable peaks should be very useful for various HSQC-based titration experiments. It also makes CP-HISQC a potentially useful template for ^{15}N R_2 experiment, PRE experiment, and other similar measurements.

In addition to superior spectral resolution, CP-HISQC experiment also offers reasonably good sensitivity. This can be appreciated by looking at A3 resonance which is labeled in the spectral map. The signal-to-noise ratio for this peak, which belongs to the U subspectrum, is 85:1 (see Fig. 3c, side panel). This is comparable to the S/N ratio found in the SOFAST-HMQC spectrum, 123:1 (Fig. 3d, side panel).

To further characterize the sensitivity of the two experiments, we have selected 22 peaks belonging to the U subspectrum which are well resolved and can be unambiguously assigned in all of the spectra (Zhang et al. 1994) (the assignment is shown in Fig. S1). For each of these spectral peaks we have determined the signal-to-noise ratio. The results are shown in Fig. 4a, where the x axis represents the intensity of CP-HISQC signals, while the y axis represents the *relative* intensity of CP-HISQC with respect to SOFAST-HMQC. On

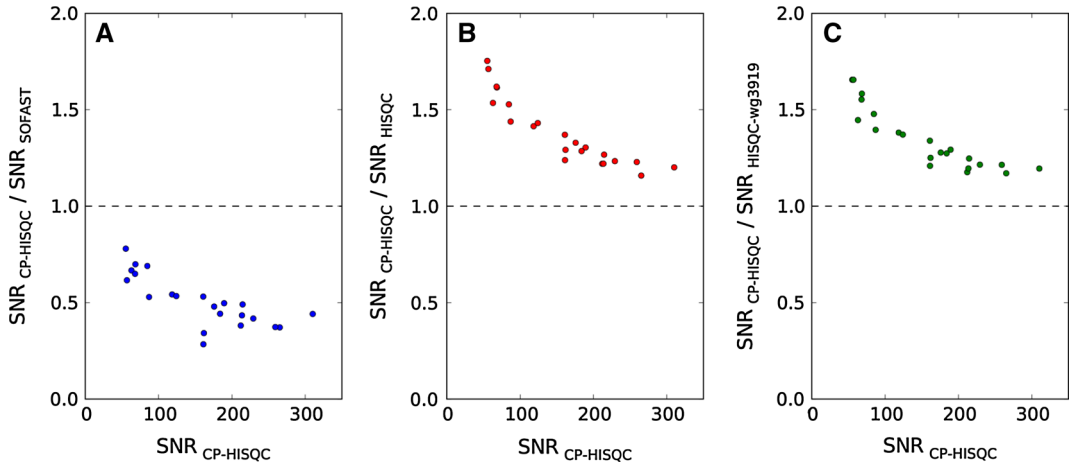

Fig. 4 Sensitivity of CP-HISQC experiment relative to SOFAST-HMQC, regular HISQC, and HISQC-wg3919 experiments (**a**, **b**, and **c**, respectively). Plotted along x axis: signal-to-noise ratio (SNR) of the individual peaks in the U subspectrum of CP-HISQC spectrum of drkN SH3. Plotted along y axis: relative signal-to-noise ratio of the same peaks, as obtained from comparison with other experiments. The SNR values are calculated using peak intensities (i.e. fitted maximum amplitudes), normalized by the noise level

average, the sensitivity of the CP-HISQC experiment proves to be 0.51 of that achieved by SOFAST-HMQC. It is worth noting, however, that CP-HISQC becomes increasingly competitive for the weaker signals (cf. the negative correlation in Fig. 4a). For the weakest peak, that from residue S10, the sensitivity of the CP-HISQC experiment relative to SOFAST-HMQC reaches 0.78.

A similar comparative analysis can be performed for the peaks from the F subspectrum. For the most part the F peaks are insensitive to exchange and therefore have much higher intensity than U peaks. Using the data from 44 well-resolved F resonances, we have found that the relative sensitivity of CP-HISQC compared to SOFAST-HMQC on average amounts to 0.36. In the case of surface residue N35, which experiences fast solvent exchange, this parameter rises to 0.57. In this connection it should be noted that CP-HISQC experiment has been designed to target U sites rather than well-protected F sites. At the same time, SOFAST-HMQC is known to be very efficient for F species, i.e. small globular proteins.

Of note, standard experiments such as SOFAST-HMQC cannot be easily optimized for simultaneously collecting data from U and F components at or near physiological conditions. Indeed, in U species the $2N_xH_x$ mode which is employed in SOFAST-HMQC undergoes rapid decay due to solvent exchange, $k_{ex} \sim 15–150\ s^{-1}$. On the other hand, in F species this mode is relatively long-lived, $R_{DQ/ZQ} \sim 1–5\ s^{-1}$ assuming the temperature 30–37 °C. This imposes conflicting requirements on the length of the t_1 evolution period. The new CP-HISQC experiment is free of this complication. Recall that CP-HISQC utilizes the N_x mode which decays slowly in both U and F species.

Of major interest to us is the contribution of the CP element. Figure 4b illustrates the sensitivity of CP-HISQC experiment relative to the previously reported HISQC experiment. For those U peaks that are well resolved and unambiguously assigned, the average increase in sensitivity proves to be 1.38. The most significant gain, 1.75, is again observed for the weakest peak, S10.

In part, these gains are due to the more efficient water preservation scheme implemented in CP-HISQC. To quantify this factor, we have implemented the reference experiment HISQC-wg3919. The only difference between CP-HISQC and HISQC-wg3919 is that the former starts with CP element, while the latter relies on refocused INEPT. The relative sensitivity of the two measurements is illustrated in Fig. 4c. The average gain from the use of the CP element is described by the factor 1.34.

Finally, CP element also works well for F species. All of the 44 selected F peaks are stronger in the CP-HISQC spectrum than in the HISQC-wg3919 spectrum. On average, the improvement is expressed by the factor 1.10. The biggest gain, 1.38, is again found in residue N35.

Based on all of the above, we suggest that CP-HISQC is the best choice of experiment for $^{1}H^{N}–^{15}N$ spectroscopy of drkN SH3 at or near physiological conditions. The HISQC scheme achieves critical improvement in resolution, whereas the CP element offers significant boost in sensitivity.

Discussion

The efficiency of CP scheme: dependence on τ_{mix}

The advantage of CP-HISQC over more conventional schemes, such as HSQC, FHSQC, SOFAST-HMQC, stems from three factors:

(i) The reliance on the in-phase N_x evolution during the t_1 period. It is well appreciated that N_x has more favorable relaxation properties compared to $2N_xH_z$ or $2N_xH_x$ (Bax et al. 1990). In the context of this study it is especially important that N_x is immune to the effects of solvent exchange, whereas $2N_xH_z$ and $2N_xH_x$ suffer heavy losses (Iwahara et al. 2007).[2]

(ii) The ability of the CP element to efficiently utilize the influx of H_x magnetization from the H_2O proton pool, converting H_x into the desired N_x magnetization.

(iii) The more favorable properties of the CP element relative to the INEPT scheme with regard to spin relaxation (Levitt 1991) as well as solvent exchange. Both CP and refocused INEPT generate multispin modes on the route from H_x to N_x. However, the refocused INEPT has a higher content of multispin modes and, therefore, suffers greater losses due to solvent exchange.

The advantages associated with property (*i*) have been previously documented, although to the best of our knowledge the application to backbone amides undergoing fast solvent exchange is new. This aspect is also illustrated above (cf. the sharpening of spectral peaks in the HISQC family of spectra, Figs. 2 and 3). Therefore in what follows we focus on properties (*ii*) and (*iii*) wherein lies the novelty of our approach.

To analyze the details of CP transfer in the presence of fast solvent exchange we have conducted a series of numeric simulations. The results are presented in Figs. 5, 6, 7, 8 below. Briefly, we have simulated the behavior of the two-spin system, $^1H^N$–^{15}N, undergoing exchange with the large water proton pool. For simplicity, we have neglected (dipolar and CSA) relaxation. Other aspects, such as DIPSI-2 pulse train which is applied on-resonance or close to resonance with $^1H^N$ signal but off-resonance relative to the water line, are modeled in a fully realistic fashion. In Fig. 5 we analyze the efficiency of the CP transfer, i.e. the amount of the generated N_x magnetization, as a function of the mixing time τ_{mix}. Since the focus of this simulation is on the CP element, water preservation outside the CP element is of no interest at this point. Accordingly, we disregard the synchronization condition $\tau_{mix} = (n/2) \times T_{DIPSI2}$.

[2] In principle, loss of multispin correlations due to solvent exchange can also be described as "relaxation". However, we prefer to reserve this term for faster processes—specifically for the dynamic regime where $J_{NH}/k_{ex} \leq 1$ (including Redfield limit where $J_{NH}/k_{ex} \ll 1$ and the formula for scalar relaxation of the first kind applies (Abragam 1961)). Since in our study these conditions are not necessarily fulfilled we prefer a more general description referring to the "loss of multispin correlations due to solvent exchange" (Skrynnikov and Ernst 1999). In what follows the term "relaxation" refers to dipolar and CSA mechanisms.

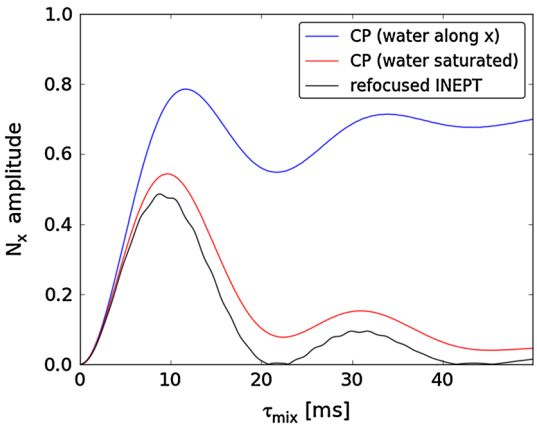

Fig. 5 Numerical simulations of proton-to-nitrogen magnetization transfer using CP or refocused INEPT element in the presence of solvent exchange with $k_{ex} = 100\ s^{-1}$. The simulations model the conditions and setup of the actual backbone experiment, including the use of DIPSI-2 sequence with $\nu_1^H = \nu_1^N = 4.0$ kHz and proton *rf* carrier positioned on-resonance with $^1H^N$ spin at 8.2 ppm (see "Materials and Methods" for additional details). Water magnetization is assumed to be initially aligned along x (*blue* and *black profiles*) or otherwise saturated (*red profile*). The refocused INEPT is assumed to be slightly asymmetric, $\tau_a/\tau_b = 0.9$, same as in the experimental measurement

Shown in Fig. 5 are three different profiles. The blue curve corresponds to the CP element as implemented in our experiment. Initially it is assumed that full amount of ^1H magnetization is available both on the amide and the water protons. Water ^1H magnetization is first aligned along the x axis and then effectively locked by the DIPSI-2 train. The resulting transfer profile is very different from the conventional $(1/2)(1–\cos(\pi J_{HN}\tau_{mix}))$ oscillatory pattern normally associated with the cross-polarization transfer. As can be seen from the plot, the transfer efficiency actually converges toward the plateau value of ca. 0.70. This behavior can be understood by noticing that fresh proton magnetization is constantly injected into the amide site via solvent exchange and then transformed into N_x. After sufficiently long τ_{mix} the system reaches a state of quasi equilibrium, $H_x \rightleftarrows 2(H_yN_z + H_zN_y) \rightleftarrows N_x$, where the loss of H_yN_z, H_zN_y due to solvent exchange is compensated by continuous influx of H_x from the large water pool.

The maximum transfer efficiency 0.79 is achieved with τ_{mix} of 11.6 ms. This is somewhat longer than the standard duration of the cross-polarization period, $\tau_{mix} = 1/J_{HN} =$ 10.8 ms. The additional time is required to utilize a portion of the incoming water polarization, maximizing the output of N_x. Note, however, that transfer efficiency remains very good in a broad range of τ_{mix}, from ca. 10 to ca. 13 ms. This provides us with the freedom to adjust τ_{mix} such as to satisfy the synchronization condition (see Fig. 1 and surrounding discussion). The distinctive dependence on τ_{mix}

as seen in Fig. 5 has been verified experimentally (shown in what follows).

The red profile in Fig. 5 describes the situation which is in every way similar, except it is assumed that water magnetization is saturated and remains zero throughout the course of the CP period. This scenario leads to a rather different outcome. Initially, amide magnetization H_x is transformed into N_x, with maximum transfer efficiency 0.54 reached at $\tau_{mix} = 9.6$ ms. As mixing time is increased beyond this level, amide $^1H^N$ magnetization is nullified due to the exchange with saturated water magnetization. Furthermore, the existing N_x magnetization is transformed back into H_x and subsequently destroyed through solvent exchange. As a result, the efficiency of the transfer drops to a very low level.

Finally, the black profile in Fig. 5 corresponds to the refocused INEPT transfer, where $\tau_{mix} = 2\tau_a + 2\tau_b$. In this case the behavior of water magnetization is different and deserves a special discussion. During the delays τ_a both amide and water ^1H magnetizations undergo free precession. Their precession frequencies are different by several thousand Hz. As a result, when water magnetization enters the amide site, it does so with a random phase (relative to the amide magnetization). Consequently, the input from water magnetization cancels out and the situation becomes generally similar to the previous scenario, where water signal is saturated.[3]

What are the main lessons that can be learned from Fig. 5? Clearly, the biggest advantage associated with CP sequence stems from its ability to utilize water magnetization (blue curve). If water signal is saturated, the performance of the CP scheme deteriorates (red curve). In fact, the efficiency of the CP element becomes comparable to that of the refocused INEPT (black curve). Hence it is mostly the water magnetization which makes the CP element successful, cf. factor (*ii*) in the above list.

At the same time we note that CP element is less susceptible to the exchange losses than refocused INEPT, corresponding to factor (*iii*) in the above discussion. This becomes apparent from the comparison of red and black profiles in Fig. 5. In both simulations there is no influx of magnetization from water, yet CP holds an advantage since it is less affected by the loss of $2H_yN_z$ and $2N_yH_z$. This advantage, however, is not as significant as the gain from water magnetization. Therefore we conclude that it is mainly factor (*ii*) which makes CP scheme superior, whereas factor (*iii*) plays a smaller role. This observation holds true for the entire range of k_{ex} rates relevant to our experiment.

[3] This general discussion is also valid in the situation when INEPT element includes pulsed field gradients.

What are the ramifications of the results in Fig. 5 for the pulse sequence Fig. 1 and possible alternative schemes?

First, it is worth noting that refocused INEPT element does not need to be symmetric. In fact, the first half of the refocused INEPT, $H_x \rightarrow 2H_yN_z$, is more vulnerable to solvent exchange than the second half, $2N_yH_z \rightarrow N_x$. Indeed, in the context of the INEPT scheme H_x, $2H_yN_z$, and $2N_yH_z$ are all effectively destroyed by solvent exchange, whereas N_x remains unaffected. Additional simulations establish that asymmetric INEPT using $\tau_a/\tau_b = 0.9$ shows a slightly better performance, with transfer efficiency increased by ca. 1 %. Generally, it is common to use somewhat different settings for τ_a and τ_b in the refocused INEPT, and we follow this path both in our experimental measurements and in numeric simulations.

Second, the conventional INEPT scheme can be modified such as to effectively lock water magnetization and utilize it toward generating N_x. Specifically, this can be accomplished by means of CPMG-INEPT (Muller et al. 1995; Mulder et al. 1996) with sufficiently high pulse repetition rate. We have simulated such hypothetical experiment and found that is indeed more sensitive than its conventional counterpart. However, the improvement proves to be limited, well below the level achieved by the CP scheme. This can be readily understood by noticing that CPMG-INEPT is useful only with regard to $H_x \rightarrow 2H_yN_z$ transfer, i.e. as first half of the refocused INEPT, but does not contribute anything during the second half. Therefore, we have not pursued this idea any further.

Third, we have considered the idea of a pulse sequence using two CP elements (for direct and reverse transfer). Relying on CP element to transfer magnetization from ^{15}N to ^1H has only limited advantages. Indeed, in this case water magnetization cannot be used to boost the signal. On the other hand, CP element remains less susceptible to exchange losses, cf. factor (*iii*) in the preceding discussion. In principle, this property offers ca. 10–15 % gain in observed signal (see Fig. 5) in addition to what has been achieved in the current CP-HISQC experiment. However, in practice the design using two CP elements is problematic. In particular, inserting CP element prior to the acquisition period makes it difficult to preserve water magnetization while at the same time minimizing residual water signal. Furthermore, second CP element increases the load on the probe, possibly requiring longer recycling delays. Considering these complications, we did not make any attempt to implement such experiment.

The efficiency of CP scheme: dependence on k_{ex}

Amide exchange rates in disordered proteins are dependent on primary sequence. As a result, an IDP sample presents a spectroscopist with relatively broad range of k_{ex} values. If

the sample also includes partially or fully folded components, as is the case with drkN SH3, then there is an additional set of signals with very low k_{ex}. Generally one may expect to encounter the situation where the peaks in the spectrum show a range of k_{ex} extending from 0 to $\sim$200 s^{-1}. Ideally, all of these peaks should be captured in a single experiment. As it turns out, the CP scheme can effectively deal with this situation: one τ_{mix} setting is sufficient to capture all resonances with near-optimal sensitivity. Specifically, the consensus setting $\tau_{mix} = 10.7$ ms achieves transfer efficiency within 6 % of the optimal level over the entire range of k_{ex} rates. The refocused INEPT scheme is somewhat less forgiving, i.e. a single τ_{mix} value cannot accommodate the range of k_{ex} values quite as well.

The range of k_{ex} rates from 0 to ca. 200 s^{-1} is generally suitable for $^{1}H^{N}$–^{15}N spectroscopy. In this region the advantage of the CP element over refocused INEPT is expressed by the average factor 1.5 (see Fig. 6). The area outside this region is more problematic from the perspective of $^{1}H^{N}$–^{15}N spectroscopy. For solvent exchange rates exceeding 500 s^{-1} refocused INEPT becomes completely inefficient, although CP element retains a reasonably good performance. In what follows we investigate the performance of CP element on the sample of Sos at elevated temperature where k_{ex} reaches 620 s^{-1}. It is demonstrated that even under these extreme conditions it is possible to obtain CP transfer with ca. 70 % efficiency (although this requires the use of longer mixing times).

We have also conducted spin dynamics simulations for Lys NH_3 groups. The results were found to be similar to those shown in Fig. 6, suggesting that CP element should be equally useful in the context of lysine side-chain experiments (Iwahara et al. 2007). As a caveat, note that the maximum transfer efficiency in this four-spin system cannot exceed 44 % (this limit holds for both refocused INEPT and CP schemes).

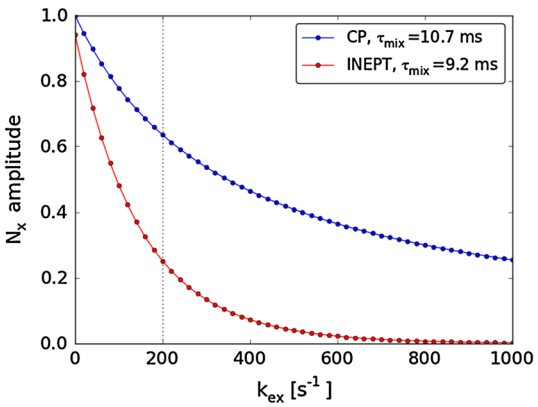

Fig. 6 The efficiency of CP element versus refocused INEPT transfer as a function of amide solvent exchange rate k_{ex}. The simulation parameters, including τ_{mix} settings, are the same as used in the actual experimental measurements (see "Materials and Methods")

The efficiency of CP scheme: dependence on *rf* field settings

Two conditions need to be met in order to achieve high efficiency of the CP element: (i) cross-polarization transfer per se should be effective, i.e. amide proton magnetization should be locked and fulfill Hartmann-Hahn condition, $\nu_1^H = \nu_1^N$, and (ii) water magnetization should be effectively locked along the same axis as amide proton magnetization. Both requirements could be readily satisfied if infinitely strong *rf* fields were available. In practice, however, ν_1^N is subject to rather stringent technical limitations, which automatically puts a limit on ν_1^H $(= \nu_1^N)$. As a consequence, ν_1^H is actually comparable to the offset Δ between the amide $^{1}H^{N}$ resonances and the water signal.

To address this aspect of the problem we have conducted a series of numeric simulations. In particular, the simulated data shown in Fig. 7a (red curve) imitate the conditions of our drkN SH3 experiment. In these simulations we assume that proton *rf* carrier is placed in the middle of the amide region, 8.2 ppm, such that the offset relative to that water signal is 3.5 ppm ($\Delta = 2.1$ kHz). We further assume that the strength of the DIPSI–2 *rf* field is $\nu_1^H = 4.0$ kHz and the solvent exchange rate is $k_{ex} = 100$ s^{-1}. Using this set of parameters we have calculated the CP "excitation profile", i.e. determined the amount of N_x magnetization generated by the CP element for the range of $^{1}H^{N}$ chemical shifts. As it turns out, the entire amide region extending from 7.2 to 9.2 ppm is covered in a fairly uniform fashion (red curve in Fig. 7a). Somewhat higher efficiency is achieved at the upfield end of the spectrum compared to the downfield end, 0.80 vs. 0.72. This observation can be readily understood. Recall that CP transfer is efficient when amide and water magnetization are both locked along the x axis. This is easier to achieve for $^{1}H^{N}$ magnetization precessing at 7.2 ppm than for $^{1}H^{N}$ magnetization precessing at 9.2 ppm.

For the problem at hand the following relationship always holds true: $\nu_1^H, \Delta \gg k_{ex}$.Under this condition it can be shown that the efficiency of the CP element depends on the dimensionless ratio ν_1^H/Δ.[4] Figure 7b shows how the efficiency of CP transfer changes with the increase in ν_1^H/Δ. It is clearly desirable to use stronger *rf* fields in order to boost the sensitivity of the experiment. The inspection of the simulated data in Fig. 7b suggests that $\nu_1^H/\Delta \sim 2.0$ should be considered a reasonable target for CP-HISQC

[4] This parameter is the same as $\tan\theta$, where θ is the standard tilt angle.

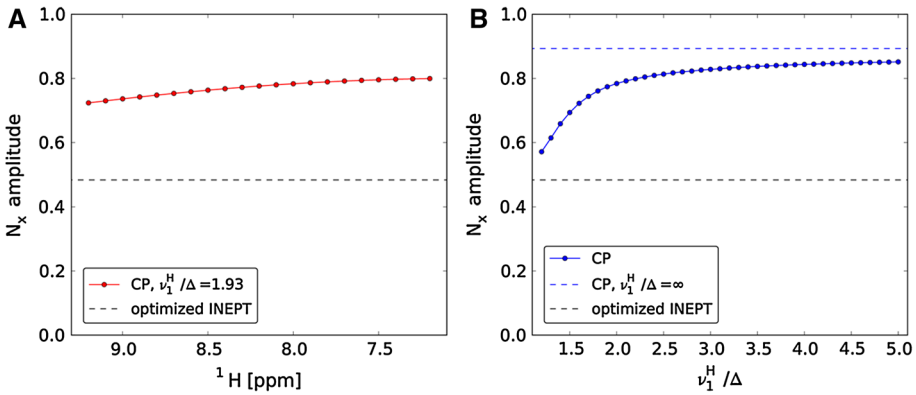

Fig. 7 The efficiency of CP element for backbone amides as a function of (**a**) $^{1}H^{N}$ chemical shift and (**b**) the strength of *rf* field used in CP mixing, $\nu_1^H(=\nu_1^N)$, relative to the offset between the proton carrier and the water signal, Δ. The simulations assume DIPSI-2 mixing with $\tau_{mix} = 10.7$ ms, proton *rf* carrier positioned at 8.2 ppm, and $k_{ex} = 100\ s^{-1}$. The results in (**b**) additionally assume that proton *rf* carrier is on-resonance with $^{1}H^{N}$ spin

measurements. Increasing the strength of *rf* field beyond this level produces only marginal improvement (cf. the curve in the graph which levels off and converges toward the plateau). In our experimental study of drkN SH3 the parameter ν_1^H/Δ was 1.93. The corresponding CP excitation profile is shown in Fig. 7a. In the study of the Sos peptide ν_1^H/Δ was 2.70 since $^{1}H^{\varepsilon}$ resonates closer to the water resonance and hence the offset Δ is smaller.

As already indicated, the limiting factor in setting up the CP-HISQC experiment is the nitrogen *rf* power. Excessive power leads to sample heating and may cause probe arcing (Keifer 1999) which severely degrades the performance of the pulse sequence. In the worst-case scenario, the probe can be permanently damaged. In our drkN SH3 measurements we have applied $\nu_1^N = \nu_1^H = 4.0$ kHz for 10.7 ms and found these settings to be safe. To quantify the amount of heating, we have prepared the sample where the coaxial insert tube was filled with methanol. This sample has been used to determine the temperature during the course of the CP-HISQC experiment as recently described (Yuwen and Skrynnikov 2013). The sample heating proved to be modest, 0.4 °C. Roughly half of the effect comes from the CP element, whereas the other half is due to proton decoupling during t_1. We have repeated these measurements on a sample additionally containing 100 mM NaCl and found that in this case the temperature increased by 0.8 °C. If necessary, one can compensate for such heating effects by adjusting the setting of variable-temperature unit.

It is worth noting that the problems associated with *rf* power are greatly alleviated in the latest-generation probes (Ban et al. 2012). The new probes can easily meet and surpass the $\nu_1^H/\Delta = 2.0$ condition. This is true not only for 500–600 MHz spectrometers, but also for higher field machines. The sample heating remains modest, even for high-salt samples, which can be attributed to the improvements in probe head design.[5] There is also an additional benefit from using stronger *rf* fields during the CP period as it helps to preserve water magnetization (see next section). All of this augurs well for future applications of the CP-HISQC experiment.

Next let us turn to the question of the proton carrier setting. From the perspective of Hartmann-Hahn transfer, it is advisable to set proton *rf* carrier in the middle of the amide region, at around 8.2 ppm. On the other hand, to simultaneously lock amide and water magnetization one may prefer to place the carrier between the two respective signals, at around 6.5 ppm. Which choice is better from the standpoint of the overall transfer efficiency? The simulations demonstrate that 8.2 ppm is very close to an optimal choice. A small improvement can be obtained by slightly shifting the carrier toward water. For $\nu_1^H/\Delta = 2.00$ this improvement becomes inconsequential (0.2 %). Therefore, we advocate 8.2 ppm, corresponding to the middle of the $^{1}H^{N}$ spectral region, as a standard choice for proton carrier setting.

Finally, let us touch upon the issue of pulse calibration. Significant miscalibration of the DIPSI-2 proton pulse reduces the efficiency of the Hartmann-Hahn transfer and, in addition, has an adverse effect on water preservation. Nevertheless, a small amount of error is well tolerated—deliberately mis-setting DIPSI-2 pulses by ±2 μs (3 %) causes virtually no change in the performance of CP-

[5] With this new hardware it is likely possible to execute the CP-HISQC experiment with shorter recycling delays. If in addition one can speed up the recovery of water magnetization, e.g. by introducing paramagnetic water relaxation agents (Hiller et al. 2005; Theillet et al. 2011), this can further improve the sensitivity of the CP-HISQC experiment. One should be mindful, however, that relaxation agents may perturb a delicate conformational equilibrium in the sample of an IDP.

HISQC. While it is recommendable to use HSQC-based sequence to calibrate proton pulses, it is also fine to use the standard water-based calibration procedure.

Preserving water magnetization

For labile protons in our drkN SH3 experiment solvent exchange rates mostly fall in the range 15–150 s^{-1}. On the other hand, the duration of the recycling delay d_1 is 1.0 s. Under these conditions, it is clear that amide $^1H^N$ magnetization is completely replaced with water magnetization during d_1 and therefore the optimal length of the recycling delay is dictated by recovery of water (rather than the relaxation properties of $^1H^N$). Consequently, it is important to prevent water saturation during the pulse sequence[6] and instead preserve water magnetization, such as to avoid long recovery periods.

CP-HISQC sequence is designed such as to ensure good water preservation properties. First, water magnetization is placed along the x axis by hard ^1H pulse.[7] Then it is effectively locked by a train of DIPSI-2 pulses, all of which have phase x or −x. After that water magnetization is returned to the z axis prior to application of the pulsed field gradient. Note that this scheme is subject to certain requirements regarding the synchronization of τ_{mix} with T_{DIPSI2} and the choice of ν_1^H, which have already been discussed above. The same tactics is used during the t_1 period, where the water is first placed along x, then effectively locked by the train of (on-resonance) WALTZ pulses with phase x (−x), and after that returned to z axis. Finally, during the refocused INEPT period, the effort is made to keep water magnetization along the z axis. The success of the water-preservation strategy can be conveniently characterized by the so-called water flip-back ratio *f*, which compares water magnetization before and after each scan, $f = M_{z,H2O}^{after}/M_{z,H2O}^{before}$ (Hiller et al. 2005).

We have determined the value of *f* for different experimental sequences used in this study (all measurements were conducted on the sample of Sos at 30 °C). In doing so we followed the procedure described by Hiller and co-workers. Considering 1D version of the experiments (i.e. t_1 set to zero) we have found that FHSQC and SOFAST-HMQC boast flip-back ratio *f* of 97 and 98 %, respectively. Given that these sequences preserve water magnetization so nicely, they can be executed with very short recycling delays. On the other hand, the HISQC-family sequences do not fare as well, with $f = 0.89$ found in the original HISQC, 0.93 in HISQC-wg3919, and 0.94 in CP-HISQC. These values typically require recycling delays on the order of 1 s. For $f = 0.94$ and $d_1 = 1$ s it is easy to estimate that CP-HISQC experiment reaches the steady state where ca. 75 % of the equilibrium water magnetization are available prior to each scan (Hiller et al. 2005). This result has been confirmed by additional experimental measurements (not shown).

Note that the coefficients *f* show substantial dependence on t_1. For instance, in the CP-HISQC experiment water magnetization experiences certain loss while being locked by WALTZ pulse train during t_1 period. For long t_1 evolution time, $t_1 = 175$ ms, this loss amounts to ca. 15 %. Therefore the *f* values derived from 1D experiments may not be ideally suited to determine the optimal recycling delays. As an alternative, we have recorded several trial 2D spectra and thus determined the d_1 values which ensure (near) optimal S/N ratio. Based on this standard procedure, the interscan delay was set to 0.2 s for SOFAST-HMQC and FHSQC experiments, while it was set to 1.0 s for HISQC, HISQC-wg3919, and CP-HISQC. All of these settings are consistent with the duty cycle requirements.

Finally, in all of our measurements we have used external lock, with D_2O added into coaxial insert tube (Wilmad, WGS-5BL). Conversely, adding D_2O directly to the protein sample in the presence of fast solvent exchange may cause a number of undesirable effects (Yuwen and Skrynnikov 2013).

CP transfer for amides with very fast solvent exchange

In the previous sections we have demonstrated that HSQC-style scheme can be used with the samples where solvent exchange rates k_{ex} approach 200 s^{-1}. Above this threshold, however, HSQC-type experiments become impractical because of extensive line broadening and loss of magnetization during the transfer steps. This is especially relevant for Lys and Arg side chains, where solvent exchange at pH 7.4, 37 °C is exceedingly fast. Many of the backbone $^1H^N$–^{15}N sites also suffer from very fast solvent exchange under physiological conditions.

In this situation one may opt for an alternative sequence design, different from a regular HSQC-like scheme. Specifically, let us consider a design where magnetization transfer starts from $^1H^N$, whereas detection is done on another spin, such as $^1H^\alpha$ or $^{13}C'$ (Bermel et al. 2009; Novacek et al. 2011; Gil et al. 2013). In what follows, we demonstrate that CP-based transfer $H_x \rightarrow N_x$ is well suited for use in any such sequence. In fact, the CP element

[6] Note that in the case of (fully or partially) folded proteins the saturation of the water signal does not only hurt labile $^1H^N$ protons, but also those protons that are protected from solvent exchange. Specifically, the saturation is transferred via spin diffusion from solvent-exposed protons on the surface of the protein to protons in the hydrophobic core, thus reducing the amount of magnetization across the board.

[7] Of interest, certain advanced schemes exist to align water magnetization along the effective *rf* field (Hansen and Kay 2007). These schemes, however, are only useful for spin-lock experiment and do not help in the case of phase-alternated pulse trains such as DIPSI-2.

proves to be indispensable if the spectra are to be recorded in the presence of very fast solvent exchange. Indeed, the simulations shown in Fig. 6 suggest that CP transfer remains fairly efficient for k_{ex} up to 1,000 s^{-1}. This is in stark contrast to INEPT which becomes totally ineffective in this regime.

In order to test these predictions experimentally, we have implemented a specialized pulse sequence for use on Arg side chains. Briefly, the magnetization transfer follows the path $H_x^{\varepsilon} \rightarrow N_x^{\varepsilon}(t_1) \rightarrow C_x^{\delta} \rightarrow H_x^{\delta}(t_2)$. The first transfer step is accomplished by means of the CP element which is identical to the one described in Fig. 1. The remaining steps are implemented in a standard fashion. The new sequence has been termed (HE)NE(CD)HD (see Fig. S2).

The (HE)NE(CD)HD spectra have been recorded on the sample of Sos peptide at pH 6.0. In addition to the data at 37 °C, we have also collected the data at 44 and 50 °C with the goal to emulate fast solvent exchange conditions observed under physiological pH. The exchange rates for Arg side-chain $H^{\varepsilon}N^{\varepsilon}$ sites were determined using the adapted version of the pulse sequence by (Segawa et al. 2008). Since the signals from four arginine residues are heavily overlapped, a single effective k_{ex} value has been obtained at each temperature: $k_{ex} = 170$, 330 and 620 s^{-1}, respectively.

Figure 8 shows the build-up of (HE)NE(CD)HD signal as a function of CP mixing time. In addition to the experimental data (circles), the plot also contains the simulated profiles (solid lines). These profiles have been calculated on the basis of the independently determined k_{ex} values, as described above. The only adjustment made in Fig. 8 involves the overall intensity scaling; other than that, no adjustable parameters have been used in generating this plot. We note that the level of agreement between the experimental and simulated data is highly satisfying.

As already pointed out, the shape of the N_x build-up profile in the presence of fast solvent exchange is different from the familiar oscillating curve. The transfer of magnetization from water to amine (or amide) proton and farther on to ^{15}N is controlled by solvent exchange, which is essentially a stochastic process. As a result, the CP build-up profiles acquire smooth character typical of stochastic processes (e.g. spin relaxation).

Note that in order to obtain efficient CP transfer, one needs to employ long τ_{mix}. Considering the data where $k_{ex} = 620$ s^{-1} (red curve in Fig. 8), the transfer efficiency ca. 50 % is achieved after 15 ms and the transfer efficiency ca. 70 % after 30 ms. This should be borne in mind if CP element is to be used in the presence of ultra-fast solvent exchange, $k_{ex} > 1{,}000$ s^{-1}. In this case the need for long τ_{mix} may constitute a technical limitation because of potential probe heating problem. Note also that in the case of long τ_{mix} one has to reckon with partial loss of water magnetization during the mixing period (in part due to saturation transfer from protein to water).

Also shown in Fig. 8 are the data from (HE)NE(CD)HD experiment where the starting CP element is replaced with

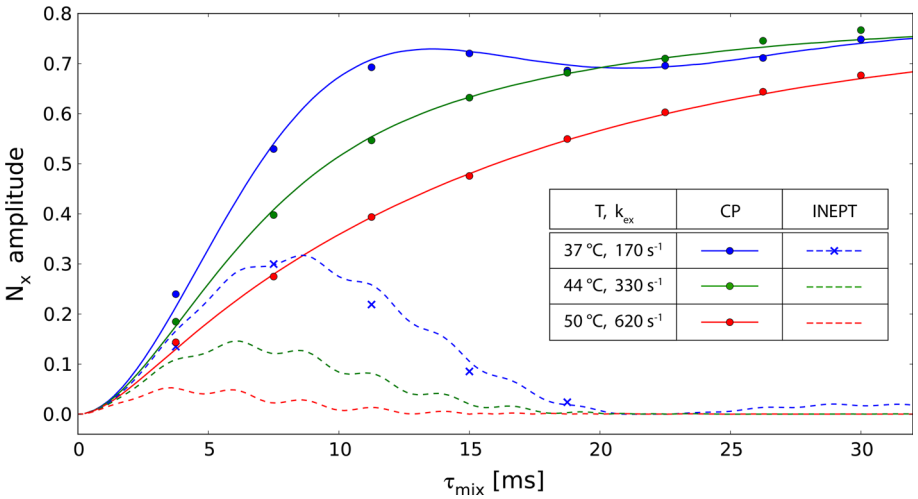

Fig. 8 The efficiency of CP transfer vs. INEPT transfer in a system with very fast solvent exchange (arginine side-chain $N^{\varepsilon}H^{\varepsilon}$ sites in Sos peptide). The experimental data have been collected using (HE)NE(CD)HD sequence employing proton-to-nitrogen CP element (*circles*) or, alternatively, refocused INEPT (*crosses*). The experiment was executed in 1D mode; the efficiency of the transfer has been estimated based on the intensity of the signal which represents four (overlapped) H^{δ} resonances. The solvent exchange rates k_{ex} listed in the legend have been measured independently using the suitably adapted version of the experiment by (Segawa et al. 2008). Also shown are the results of numeric simulations for CP and refocused INEPT transfer (continuous and dashed lines, respectively). To enable the comparison between the experiment and the simulations, the overall intensity scaling has been applied to the data. Specifically, for all data recorded at 37 °C, including both CP and INEPT data, the signal intensities have been multiplied by a constant scaling factor. This factor has been adjusted such as to match the simulated profile. The same procedure has been used for the data collected at two other temperatures

a regular refocused INEPT. The experimental data obtained at 37 °C are indicated by blue crosses; the simulated data pertaining to three different temperatures are shown as dashed curves. Clearly, the efficiency of INEPT transfer in the presence of very fast solvent exchange is low. For instance, in the case where $k_{ex} = 620\ s^{-1}$ the efficiency of the INEPT transfer is meager 5 % (red dashed curve in the plot Fig. 8). Obviously, it is not practical to use ^{1}H-to-^{15}N or ^{15}N-to-^{1}H INEPT transfer under very fast solvent exchange conditions.

Measurements targeting arginine, lysine, and histidine side chains, including side-chain sites undergoing very fast solvent exchange, play increasingly prominent role in protein NMR studies (Takayama et al. 2008; Trbovic et al. 2009; Blaum et al. 2010; Diehl et al. 2010; Esadze et al. 2011; Hu et al. 2012). The use of the CP element in this context is expected to be highly helpful.

Conclusion

Hartmann-Hahn cross-polarization in liquids is a highly efficient way of transferring magnetization. It has been shown that CP element has somewhat more favorable relaxation properties than refocused INEPT (Levitt 1991). CP transfer is also better protected against losses associated with conformational exchange (Krishnan and Rance 1995). Furthermore, CP element using DIPSI-2 significantly outperforms refocused INEPT in the presence of substantial *rf* field inhomogeneity (Majumdar and Zuiderweg 1995).

Fifteen years ago it has been shown that CP transfer is also more efficient than refocused INEPT for amide sites undergoing fast solvent exchange (Zangger and Armitage 1998). However, this observation was made in the context of a rather specialized experiment, exchange-edited HSQC. The pulse sequence developed for that purpose did not take advantage of in-phase (N_x) evolution in the indirect dimension. Also no special effort has been made to preserve water magnetization. Indeed, the role of water in the CP transfer has not been properly understood. As a consequence, the findings of that work have never found way into general-use HSQC spectroscopy. In our study we have addressed this omission by integrating the CP element into high-resolution HISQC experiment.

NMR studies of intrinsically disordered proteins are confronted with a number of significant challenges. The main difficulty arises from poor dispersion of chemical shifts in the spectra of IDPs. One should also bear in mind that the samples of IDPs often need to be prepared with low protein concentration because of the IDPs' propensity to aggregate and precipitate. Along the same lines, the measurement time is often limited because the samples tend to quickly deteriorate. If one attempts to conduct the measurements close to physiological conditions, the situation is further exacerbated by fast solvent exchange. Fast solvent exchange leads to intensity loss and dramatic line-broadening in the conventional HSQC-type spectra, making the spectroscopic studies very difficult or impossible.

In this paper we demonstrate how the complications associated with fast solvent exchange can be largely avoided and even turned into an advantage. Proton-decoupled experiment (HISQC) allows one to record the spectra with narrow peak width in ^{15}N dimension. Raising the temperature to (physiologically relevant) 37 °C achieves further sharpening of the signals in ^{15}N dimension, which effectively compensates for exchange-induced broadening in ^{1}H dimension. While the idea of proton-decoupled HSQC experiment (HISQC) is well-known, the benefits of this scheme in the context of backbone $^{1}H^{N}$–^{15}N spectroscopy of IDPs have not been previously appreciated.

The fact that water protons rapidly exchange into $^{1}H^{N}$ sites can also be used to one's advantage. First, as has been long realized, fast solvent exchange makes it possible to shorten the recycling delays. Second, as we found in this study, fast solvent exchange can be used to boost the efficiency of the CP transfer. The CP element is also a natural fit with the proton-decoupled HISQC scheme, thus leading to the CP-HISQC sequence described in this paper.

The use of the CP-HISQC scheme does not need to be limited to HSQC-style applications. This sequence can be used as a template for the experiments to measure paramagnetic relaxation enhancements (PREs), residual dipolar couplings (RDCs), etc. In particular, CP-HISQC sequence employs N_x coherence and thus it is perfectly suited for ^{15}N R_2 relaxation measurements. More broadly, the concepts used in CP-HISQC are also applicable to 3D sequences such as HNCO, HNCA, and others. Of interest, we have found that the properly designed CP element remains efficient even under very fast exchange conditions, $k_{ex} \sim 500$–$1000\ s^{-1}$. This observation suggests that proton-to-nitrogen CP transfer can be used as starting point in the pulse sequences that use non-labile ^{1}H or ^{13}C spins for detection. We have experimentally demonstrated this strategy for $H^{\varepsilon}N^{\varepsilon}$ sites in arginine side chains. Generally we believe that the pulse sequences and concepts presented in this work should significantly facilitate the spectroscopic characterization of disordered proteins at or near physiological conditions.

Materials and methods

Sample preparation

Sos peptide has been expressed in ^{13}C, ^{15}N enriched M9 media in a form of GB1-Sos fusion construct and purified by cation-exchange and gel-filtration FPLC. The peptide was

subsequently cleaved by application of formic acid (Vidovic et al. 2009) and purified by reverse phase HPLC. The concentration of the peptide has been determined by comparing the volume of V4 H^{γ} peak in 1D ^{1}H spectrum of Sos with the corresponding signal from 10 mM reference sample of valine. The conditions of the Sos sample were 1.0 mM Sos, 20 mM phosphate buffer in H_2O, pH 6.0, 0.02 % NaN_3. drkN SH3 has been expressed in ^{15}N enriched M9 media and purified according to the standard protocol (Zhang and Forman-Kay 1995). Protein concentration has been determined via UV absorbance at 280 nm. The sample conditions were 2.0 mM drkN SH3, 20 mM phosphate buffer in H_2O, pH 7.5, 0.02 % NaN_3. In both samples, Sos and drkN SH3, D_2O has been added into coaxial insert (Wilmad, WGS-5BL) to serve as external lock. This strategy avoids numerous complications that arise from use of H_2O/D_2O solvent under fast exchange conditions (Jurt and Zerbe 2012; Yuwen and Skrynnikov 2013).

NMR spectroscopy

All NMR measurements were performed on Varian Inova 600 MHz spectrometer equipped with a z-gradient TXI triple-resonance probe (after this study had been completed, CP-HISQC sequence was translated and successfully tested on Bruker DRX 500 MHz machine). 1D CP-HISQC experiment has been used to optimize *rf* field settings for the CP element. In doing so, we scanned ^{15}N power levels while maintaining ^{1}H power level fixed; we found it unnecessary to use fine power adjustments. The CP-HISQC arginine side-chain experiments on Sos have been recorded at 23, 30, and 37 °C (temperature calibrated using methanol). The spectra were collected with spectral width 6 ppm in ^{15}N dimension ($t_1 = 175$ ms) and 15 ppm in ^{1}H dimension ($t_2 = 46.5$, 23.3, and 11.8 ms for the three respective temperatures, chosen according to the formula $t_2 = 2/k_{ex}$ since the decay of the useful signal is dominated by solvent exchange, see Fig. 2). The data were apodized using phase-shifted sine-bell squared window function and zero-filled to the size 512 × 4,096. The CP-HISQC spectrum of drkN SH3 was recorded at 30 °C with spectral width 30 ppm in ^{15}N dimension and 15 ppm in ^{1}H dimension ($t_1 = 177$ ms, $t_2 = 40$ ms, chosen according to the formula $t_2 = 2/k_{ex}$ based on the compromise value $k_{ex} = 50\ s^{-1}$ for solvent exchange rate). The data were apodized and zero-filled to the size 2,560 × 4,096. The peak intensities have been obtained using nlinLS function in NMRPipe (Delaglio et al. 1995). The average noise level was estimated with the help of the function showApod. The solvent exchange rates were measured using the experiment by (Segawa et al. 2008) implemented with some minor modifications (e.g. the altered sequence evolves N_x coherence during the t_1 period instead of $2N_xC_z$).

Numerical simulations

The efficiency of proton-to-nitrogen CP and INEPT transfer in two-spin $^{1}H–^{15}N$ system has been simulated using in-house Maple and Python scripts. All coherent evolution mechanisms such as chemical shifts, *J*-couplings and *rf* pulses have been included in the simulations in a fully realistic fashion. The modeling of solvent exchange effect follows the scheme of (Skrynnikov and Ernst 1999), where all two-spin modes experience decay with the rate k_{ex}, whereas H_x^N mode exchanges magnetization with the corresponding water mode. The ratio of water magnetization to protein proton magnetization is assumed to be 1,000:1, reflecting protein concentration ca. 1 mM and assuming that a small-sized protein contains 100 exchangeable protons. The results do not change if one assumes the ratio 10,000:1, corresponding to ca. 0.1 mM sample. Given that spin relaxation in IDPs at or near physiological temperature is relatively slow and the mixing time τ_{mix} is short, we ignore dipolar and CSA spin relaxation. Likewise, we have neglected the potential effect of radiation damping noticing that water magnetization is either locked by strong *rf* field (CP) or dephased by application of pulsed field gradients (INEPT). The size of the Liouville superoperator matrix used in the simulations is 18 × 18 (comprising 15 modes from $^{1}H^{N}–^{15}N$ spin system and 3 modes from water ^{1}H spin). The initial conditions have been chosen assuming that equilibrium magnetization is available for both $^{1}H^{N}$ and water. Alternatively, we considered somewhat artificial scenario where the water is initially saturated, but $^{1}H^{N}$ retains the full amount of magnetization (see Fig. 5).

Acknowledgments This study was supported by the funds from NSF Grant MCB 1158347.

References

Abragam A (1961) The principles of nuclear magnetism. Clarendon Press, Oxford

Amezcua CA, Harper SM, Rutter J, Gardner KH (2002) Structure and interactions of PAS kinase N-terminal PAS domain: model for intramolecular kinase regulation. Structure 10:1349–1361

Bai YW, Milne JS, Mayne L, Englander SW (1993) Primary structure effects on peptide group hydrogen exchange. Proteins Struct Funct Genet 17:75–86

Ban D, Gossert AD, Giller K, Becker S, Griesinger C, Lee D (2012) Exceeding the limit of dynamics studies on biomolecules using high spin-lock field strengths with a cryogenically cooled probehead. J Magn Reson 221:1–4

Bax A, Ikura M, Kay LE, Torchia DA, Tschudin R (1990) Comparison of different modes of two-dimensional reverse-correlation NMR for the study of proteins. J Magn Reson 86:304–318

Bermel W, Bertini I, Felli IC, Piccioli M, Pierattelli R (2006) ^{13}C-detected *protonless* NMR spectroscopy of proteins in solution. Prog NMR Spectrosc 48:25–45

Bermel W, Bertini I, Csizmok V, Felli IC, Pierattelli R, Tompa P (2009) H-start for exclusively heteronuclear NMR spectroscopy: the case of intrinsically disordered proteins. J Magn Reson 198:275–281

Bista M, Freund SM, Fersht AR (2012) Domain-domain interactions in full-length p53 and a specific DNA complex probed by methyl NMR spectroscopy. Proc Natl Acad Sci USA 109:15752–15756

Blaum BS, Deakin JA, Johansson CM, Herbert AP, Barlow PN, Lyon M, Uhrin D (2010) Lysine and arginine side chains in glycosaminoglycan-protein complexes investigated by NMR, cross-linking, and mass spectrometry: a case study of the Factor H–Heparin interaction. J Am Chem Soc 132:6374–6381

Chevelkov V, Xue Y, Rao DK, Forman-Kay JD, Skrynnikov NR (2010) $^{15}N^{H/D}$-SOLEXSY experiment for accurate measurement of amide solvent exchange rates. Application to denatured drkN SH3. J Biomol NMR 46:227–244

Connelly GP, Bai YW, Jeng MF, Englander SW (1993) Isotope effects in peptide group hydrogen exchange. Proteins Struct Funct Genet 17:87–92

Croke RL, Sallum CO, Watson E, Watt ED, Alexandrescu AT (2008) Hydrogen exchange of monomeric α-synuclein shows unfolded structure persists at physiological temperature and is independent of molecular crowding in Escherichia coli. Protein Sci 17:1434–1445

Delaglio F, Grzesiek S, Vuister GW, Zhu G, Pfeifer J, Bax A (1995) NMRPipe: a multidimensional spectral processing system based on unix pipes. J Biomol NMR 6:277–293

Diehl C, Engstrom O, Delaine T, Hakansson M, Genheden S, Modig K, Leffler H, Ryde U, Nilsson UJ, Akke M (2010) Protein flexibility and conformational entropy in ligand design targeting the carbohydrate recognition domain of galectin-3. J Am Chem Soc 132:14577–14589

Esadze A, Li DW, Wang TZ, Bruschweiler R, Iwahara J (2011) Dynamics of lysine side-chain amino groups in a protein studied by heteronuclear ^{1}H-^{15}N NMR spectroscopy. J Am Chem Soc 133:909–919

Farrow NA, Zhang OW, Forman-Kay JD, Kay LE (1994) A heteronuclear correlation experiment for simultaneous determination of ^{15}N longitudinal decay and chemical exchange rates of systems in slow equilibrium. J Biomol NMR 4:727–734

Farrow NA, Zhang OW, Forman-Kay JD, Kay LE (1995) Comparison of the backbone dynamics of a folded and an unfolded SH3 domain existing in equilibrium in aqueous buffer. Biochemistry 34:868–878

Felli IC, Brutscher B (2009) Recent advances in solution NMR: fast methods and heteronuclear direct detection. ChemPhysChem 10:1356–1368

Fernandez C, Hilty C, Wider G, Guntert P, Wuthrich K (2004) NMR structure of the integral membrane protein OmpX. J Mol Biol 336:1211–1221

Gil S, Hošek T, Solyom Z, Kümmerle R, Brutscher B, Pierattelli R, Felli IC (2013) NMR spectroscopic studies of intrinsically disordered proteins at near-physiological conditions. Angew Chem Int Edit 52:11808–11812

Gray FLV, Murai MJ, Grembecka J, Cierpicki T (2012) Detection of disordered regions in globular proteins using ^{13}C-detected NMR. Protein Sci 21:1954–1960

Grzesiek S, Bax A (1993) The importance of not saturating H_2O in protein NMR: application to sensitivity enhancement and NOE measurements. J Am Chem Soc 115:12593–12594

Haddad KC, Sudmeier JL, Bachovchin DA, Bachovchin WW (2005) α-Lytic protease can exist in two separately stable conformations with different His^{57} mobilities and catalytic activities. Proc Natl Acad Sci USA 102:1006–1011

Hansen DF, Kay LE (2007) Improved magnetization alignment schemes for spin-lock relaxation experiments. J Biomol NMR 37:245–255

Hiller S, Wider G, Etezady-Esfarjani T, Horst R, Wuthrich K (2005) Managing the solvent water polarization to obtain improved NMR spectra of large molecular structures. J Biomol NMR 32:61–70

Hsu STD, Bertoncini CW, Dobson CM (2009) Use of protonless NMR spectroscopy to alleviate the loss of information resulting from exchange-broadening. J Am Chem Soc 131:7222–7223

Hu F, Schmidt-Rohr K, Hong M (2012) NMR detection of pH-dependent histidine-water proton exchange reveals the conduction mechanism of a transmembrane proton channel. J Am Chem Soc 134:3703–3713

Iwahara J, Jung YS, Clore GM (2007) Heteronuclear NMR spectroscopy for lysine NH3 groups in proteins: unique effect of water exchange on ^{15}N transverse relaxation. J Am Chem Soc 129:2971–2980

Jurt S, Zerbe O (2012) A study on the influence of fast amide exchange on the accuracy of ^{15}N relaxation rate constants. J Biomol NMR 54:389–400

Kay LE, Keifer P, Saarinen T (1992) Pure absorption gradient enhanced heteronuclear single quantum correlation spectroscopy with improved sensitivity. J Am Chem Soc 114:10663–10665

Keifer PA (1999) 90° degrees pulse width calibrations: how to read a pulse width array. Concept Magnetic Res 11:165–180

Krishnan VV, Rance M (1995) Influence of chemical exchange among homonuclear spins in heteronuclear coherence-transfer experiments in liquids. J Magn Reson A 116:97–106

Kupce E, Freeman R (1996) Optimized adiabatic pulses for wideband spin inversion. J Magn Reson A 118:299–303

Levitt MH (1991) Heteronuclear cross polarization in liquid-state nuclear magnetic resonance: mismatch compensation and relaxation behavior. J Chem Phys 94:30–38

Loh SN, Kay MS, Baldwin RL (1995) Structure and stability of a second molten globule intermediate in the apomyoglobin folding pathway. Proc Natl Acad Sci USA 92:5446–5450

Majumdar A, Zuiderweg ERP (1995) Efficiencies of double-resonance and triple-resonance J cross-polarization in multidimensional NMR. J Magn Reson A 113:19–31

Marion D, Ikura M, Tschudin R, Bax A (1989) Rapid recording of 2D NMR spectra without phase cycling: application to the study of hydrogen exchange in proteins. J Magn Reson 85:393–399

Marsh JA, Forman-Kay JD (2009) Structure and disorder in an unfolded state under nondenaturing conditions from ensemble models consistent with a large number of experimental restraints. J Mol Biol 391:359–374

Mori S, Abeygunawardana C, Johnson MO, van Zijl PCM (1995) Improved sensitivity of HSQC spectra of exchanging protons at short interscan delays using a new fast HSQC (FHSQC) detection scheme that avoids water saturation. J Magn Reson B 108:94–98

Mueller GA, Smith AM, Chapman MD, Rule GS, Benjamin DC (2001) Hydrogen exchange nuclear magnetic resonance spectroscopy mapping of antibody epitopes on the house dust mite allergen Der p 2*. J Biol Chem 276:9359–9365

Mulder FAA, Spronk CAEM, Slijper M, Kaptein R, Boelens R (1996) Improved HSQC experiments for the observation of exchange broadened signals. J Biomol NMR 8:223–228

Muller L, Legault P, Pardi A (1995) Improved RNA structure determination by detection of NOE contacts to exchange-broadened amino protons. J Am Chem Soc 117:11043–11048

Novacek J, Zawadzka-Kazimierczuk A, Papouskova V, Zidek L, Sanderova H, Krasny L, Kozminski W, Sklenar V (2011) 5D ^{13}C-detected experiments for backbone assignment of unstructured proteins with a very low signal dispersion. J Biomol NMR 50:1–11

Orij R, Postmus J, Ter Beek A, Brul S, Smits GJ (2009) In vivo measurement of cytosolic and mitochondrial pH using a pH-

sensitive GFP derivative in Saccharomyces cerevisiae reveals a relation between intracellular pH and growth. Microbiology 155:268–278

Palmer AG, Cavanagh J, Wright PE, Rance M (1991) Sensitivty improvement in proton-detected two-dimensional heteronuclear correlation NMR spectroscopy. J Magn Reson 93:151–170

Pasat G, Zintsmaster JS, Peng JW (2008) Direct ^{13}C detection for carbonyl relaxation studies of protein dynamics. J Magn Reson 193:226–232

Rucker SP, Shaka AJ (1989) Broad-band homonuclear cross-polarization in 2D NMR using DIPSI-2. Mol Phys 68:509–517

Schanda P, Brutscher B (2005) Very fast two-dimensional NMR spectroscopy for real-time investigation of dynamic events in proteins on the time scale of seconds. J Am Chem Soc 127:8014–8015

Schanda P, Kupce E, Brutscher B (2005) SOFAST-HMQC experiments for recording two-dimensional heteronuclear correlation spectra of proteins within a few seconds. J Biomol NMR 33:199–211

Segawa T, Kateb F, Duma L, Bodenhausen G, Pelupessy P (2008) Exchange rate constants of invisible protons in proteins determined by NMR spectroscopy. ChemBioChem 9:537–542

Shaka AJ, Keeler J, Frenkiel T, Freeman R (1983) An improved sequence for broad-band decoupling: WALTZ-16. J Magn Reson 52:335–338

Sklenar V, Piotto M, Leppik R, Saudek V (1993) Gradient-tailored water suppression for ^{1}H–^{15}N HSQC experiments optimized to retain full sensitivity. J Magn Reson A 102:241–245

Skrynnikov NR, Ernst RR (1999) Detection of intermolecular chemical exchange through decorrelation of two-spin order. J Magn Reson 137:276–280

Takayama Y, Castaneda CA, Chimenti M, Garcia-Moreno B, Iwahara J (2008) Direct evidence for deprotonation of a lysine side chain buried in the hydrophobic core of a protein. J Am Chem Soc 130:6714–6715

Theillet FX, Binolfi A, Liokatis S, Verzini S, Selenko P (2011) Paramagnetic relaxation enhancement to improve sensitivity of fast NMR methods: application to intrinsically disordered proteins. J Biomol NMR 51:487–495

Trbovic N, Cho JH, Abel R, Friesner RA, Rance M, Palmer AG (2009) Protein side-chain dynamics and residual conformational entropy. J Am Chem Soc 131:615–622

Vidovic V, Prongidi-Fix L, Bechinger B, Werten S (2009) Production and isotope labeling of antimicrobial peptides in Escherichia coli by means of a novel fusion partner that enables high-yield insoluble expression and fast purification. J Pept Sci 15:278–284

Werbeck ND, Kirkpatrick J, Hansen DF (2013) Probing arginine side chains and their dynamics with carbon-detected NMR spectroscopy: application to the 42 kDa human histone deacetylase 8 at high pH. Angew Chem Int Edit 52:3145–3147

Wu XD, Knudsen B, Feller SM, Zheng J, Sali A, Cowburn D, Hanafusa H, Kuriyan J (1995) Structural basis for the specific interaction of lysine-containing proline-rich peptides with the N-terminal SH3 domain of c-Crk. Structure 3:215–226

Yao SG, Hinds MG, Murphy JM, Norton RS (2011) Exchange enhanced sensitivity gain for solvent-exchangeable protons in 2D ^{1}H–^{15}N heteronuclear correlation spectra acquired with band-selective pulses. J Magn Reson 211:243–247

Yuwen T, Skrynnikov NR (2013) Proton-decoupled CPMG: a better experiment for measuring ^{15}N R_2 relaxation in disordered proteins. J Magn Reson [ePub ahead of print]

Zangger K, Armitage IM (1998) Sensitivity-enhanced detection of fast exchanging protons by an exchange-edited gradient HEHA-HA-HSQC experiment. J Magn Reson 135:70–75

Zhang O, Forman-Kay JD (1995) Structural characterization of a folded and an unfolded state of an SH3 domain in aqueous buffer and solution structure of this domain by NMR. Biochemistry 34:6784–6794

Zhang OW, Kay LE, Olivier JP, Forman-Kay JD (1994) Backbone ^{1}H and ^{15}N resonance assignments of the N-terminal SH3 domain of drk in folded and unfolded states using enhanced-sensitivity pulsed-field gradient NMR techniques. J Biomol NMR 4:845–858

Supplementary Information

CP-HISQC: a better version of HSQC experiment for intrinsically disordered proteins under physiological conditions.

Tairan Yuwen[a] & Nikolai R. Skrynnikov[a,b]*

(*a*) Department of Chemistry, Purdue University, West Lafayette IN 47907, USA
(*b*) Laboratory of Biomolecular NMR, St. Petersburg State University, St. Petersburg 199034, Russia

17 November 2013

* Corresponding author
Tel.: (765)-494 8519
E-mail: nikolai@purdue.edu

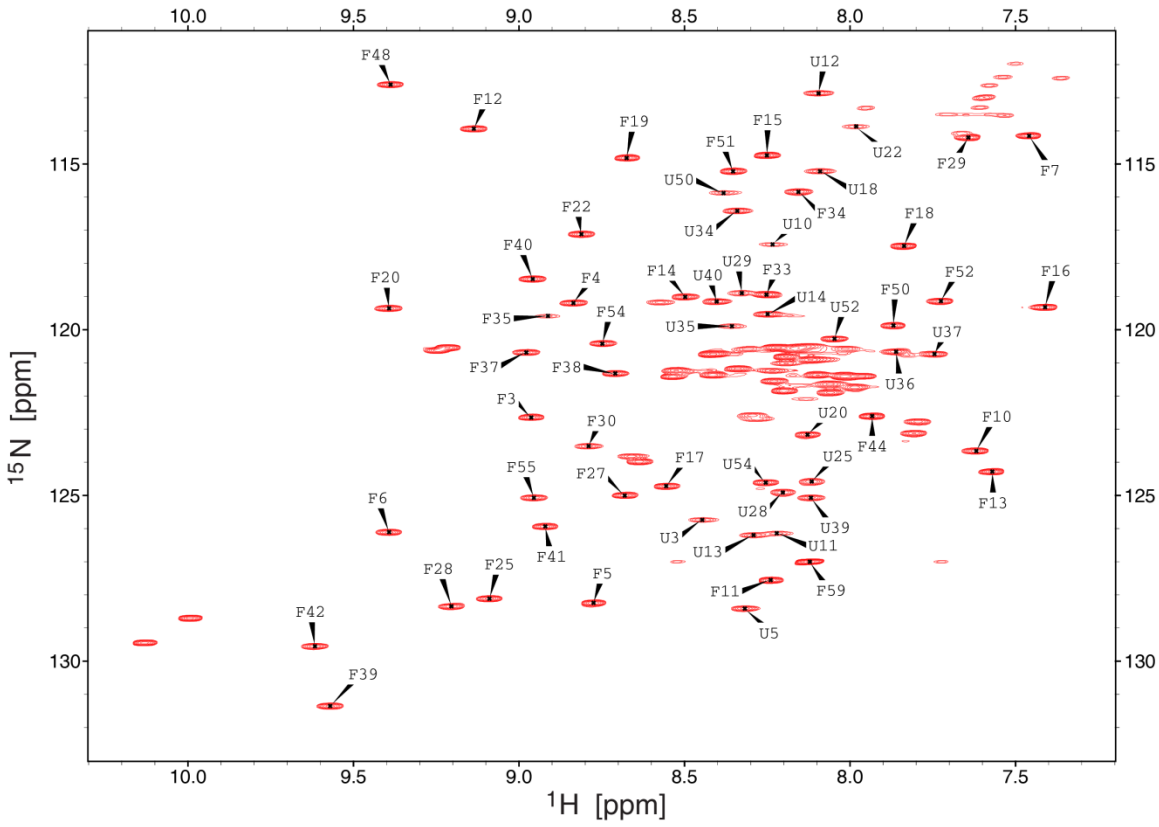

Fig. S1. CP-HISQC backbone amide spectrum of drkN SH3 (same as in Fig. 3A; sample conditions: 20 mM phosphate buffer, pH 7.5, 30 °C). The assignment is based on (Zhang et al. 1994). Only those peaks that are well-resolved and can be reliably identified in this spectrum as well as in the SOFAST-HMQC spectrum (Fig. 3B) have been selected. The F# and U# labels refer to folded and unfolded species, respectively.

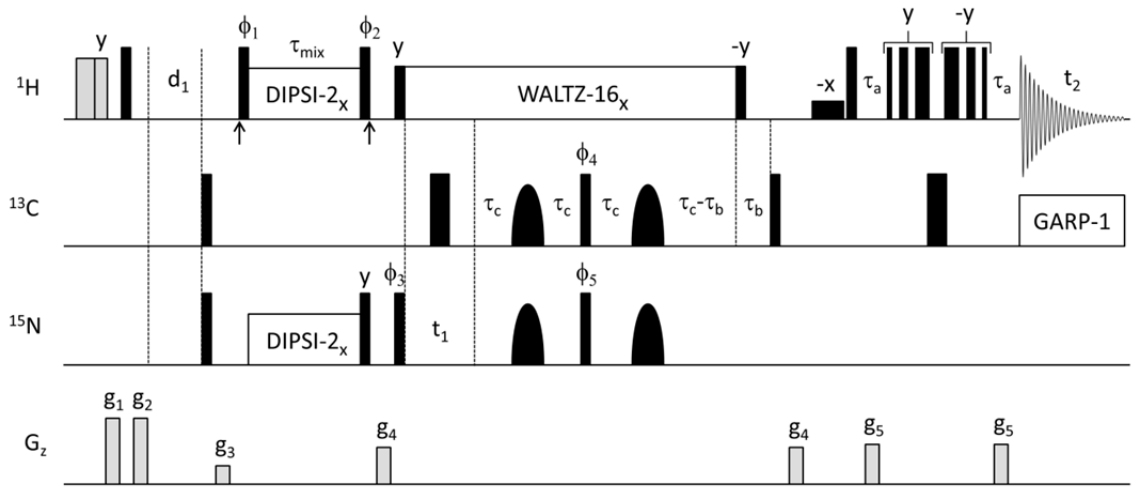

Fig. S2. (HE)NE(CD)HD sequence for recording ($^{15}N^{\varepsilon}$,$^{1}H^{\delta}$) spectral correlation map for arginine side chains. The sequence starts with the water-crusher element (Messerle et al. 1989), which is followed by long recycling delay, d_1 =3.0 s, during which the water magnetization recovers. The purpose of this design is to side-step the requirements associated with water preservation. Consequently, it becomes possible to use CP mixing period of arbitrary length, not necessarily commensurate with semi-integer number of DIPSI-2 cycles. This helps to sample the N_x build-up profiles for proton-to-nitrogen CP transfer (see Fig. 8 in the main text).

Proton carrier is set on water resonance except for the duration of the DIPSI-2 period when it is shifted to the middle of the $^{1}H^{\varepsilon}$ region, 7.2 ppm (carrier jumps are indicated by vertical arrows). Hard 90° proton pulses (5.9 μs), 90° water flip-down pulse (1.5 ms), and two water purge pulses (6.0 and 3.7 ms, *rf* field strength 12.4 kHz, indicated by shaded outlines) all have rectangular shapes. DIPSI-2 cross-polarization element (Rucker and Shaka 1989) uses 3.2 kHz *rf* field on both channels (corresponding to 90° pulses of duration 78 μs). WALTZ-16 proton decoupling (Shaka et al. 1983) and the pair of its flanking 90° pulses are applied with *rf* field strength 5.4 kHz.

Carbon carrier is positioned in the middle of $^{13}C^{\delta}$ region, at 43 ppm. Hard 90° ^{13}C pulses have the duration 16.5 μs. The selective 180° ^{13}C pulses (indicated by rounded shapes) are REBURP pulses (Geen and Freeman 1991) with peak *rf* field strength 3.1 kHz and duration 2.03 ms, offering the bandwidth of 13 ppm. GARP1 carbon decoupling is applied with *rf* field strength 1.0 kHz.

Nitrogen carrier has been set to 85 ppm. Hard ^{15}N pulses are of duration 38 μs. The selective 180° ^{15}N pulses (indicated by rounded shapes) are REBURP pulses with peak *rf* field strength 1.68 kHz and duration 4.06 ms, offering the bandwidth of 16 ppm.

The delays are $\tau_a = \tau_b = 1.80$ ms, $\tau_c = 22.0$ ms, τ_{mix} variable. The spacing between the consecutive pulses in 3-9-19 WATERGATE (Sklenar et al. 1993) is 183 μs. The phase cycle employed is: ϕ_1 = y,-y; ϕ_2 = -y,y; ϕ_3 = 2(y),2(-y); ϕ_4 = 4(x),4(-x); ϕ_5 = x; ϕ_{rec} = x,-x,-x,x,-x,x,x,-x. DIPSI-2 and WALTZ-16 sequences are applied with (initial) phase x. The TPPI scheme is implemented by inverting ϕ_5 in concert with ϕ_{rec} (Marion et al. 1989). Quadrature detection in F_1 is achieved by incrementing ϕ_5. Gradient strengths in G/cm (length in ms) are: g_1 = 20.0 (3.5), g_2 = 20.0 (2.0), g_3 = 5.0 (1.0), g_4

= 10.0 (1.0), g_5 = 11.0 (1.0). If desired, water-crusher element can be removed and τ_{mix} can be set to semi-integer number of DIPSI-2 cycles, e.g. τ_{mix} = (5/2) × T_{DIPSI2} = 22.447 ms, to improve the sensitivity of the experiment. The alternative version of (HE)NE(CD)HD sequence utilizes the refocused INEPT element instead of DIPSI-2 cross-polarization element (not shown).

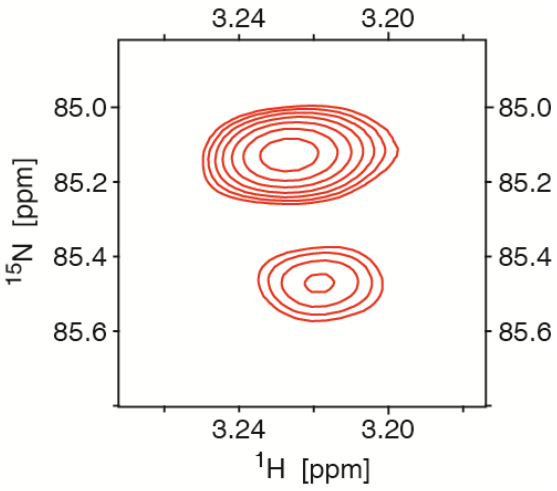

Fig. S3. ($^{15}N^{\varepsilon}$,$^{1}H^{\delta}$) spectral correlation map for Arg side chains in peptide Sos (pH 6.0, 50 ^{o}C). The spectrum was recorded using (HE)NE(CD)HD sequence with the spectral width of 2.5 ppm in ^{15}N dimension and 15 ppm in ^{1}H dimension (t_1 = 100 ms, t_2 = 100 ms). The recycling delay was d_1 =1.0 s, the net measurement time was ca. 6 min.

References

Geen H, Freeman R (1991) Band-selective radiofrequency pulses. J. Magn. Reson. 93:93-141

Marion D, Ikura M, Tschudin R, Bax A (1989) Rapid recording of 2D NMR spectra without phase cycling: Application to the study of hydrogen exchange in proteins. J. Magn. Reson. 85:393-399

Messerle BA, Wider G, Otting G, Weber C, Wüthrich K (1989) Solvent suppression using a spin lock in 2D and 3D NMR spectroscopy with H_2O solutions. J. Magn. Reson. 85:608-613

Rucker SP, Shaka AJ (1989) Broad-band homonuclear cross-polarization in 2D NMR using DIPSI-2. Mol. Phys. 68:509-517

Shaka AJ, Keeler J, Frenkiel T, Freeman R (1983) An improved sequence for broad-band decoupling: WALTZ-16. J. Magn. Reson. 52:335-338

Sklenar V, Piotto M, Leppik R, Saudek V (1993) Gradient-tailored water suppression for ^{1}H-^{15}N HSQC experiments optimized to retain full sensitivity. J. Magn. Reson. Ser. A 102:241-245

Zhang OW, Kay LE, Olivier JP, Forman-Kay JD (1994) Backbone ^{1}H and ^{15}N resonance assignments of the N-terminal SH3 domain of drk in folded and unfolded states using enhanced-sensitivity pulsed-field gradient NMR techniques. J. Biomol. NMR 4:845-858